

 Open access • Posted Content • DOI:10.1101/2020.06.16.155838

Chloroplast acquisition without the gene transfer in kleptoplastic sea slugs, *Plakobranthus ocellatus* — [Source link](#)

Taro Maeda, Shunichi Takahashi, Shunichi Takahashi, Takao Yoshida ...+16 more authors

Institutions: National Institute for Basic Biology, Japan, Graduate University for Advanced Studies, Japan Agency for Marine-Earth Science and Technology, National Institute of Genetics ...+6 more institutions

Published on: 13 Jul 2020 - bioRxiv (Cold Spring Harbor Laboratory)

Topics: Nuclear gene, Kleptoplasty, Plakobranthus ocellatus, Chloroplast and Sea slug

Related papers:

- [Chloroplast acquisition without the gene transfer in kleptoplastic sea slugs](#)
- [Transcriptomic Evidence for the Expression of Horizontally Transferred Algal Nuclear Genes in the Photosynthetic Sea Slug, *Elysia chlorotica*](#)
- [Horizontal gene transfer of the algal nuclear gene psbO to the photosynthetic sea slug *Elysia chlorotica*.](#)
- [The Chloroplast and Photosynthetic Eukaryotes](#)
- [Expression of the Nucleus-Encoded Chloroplast Division Genes and Proteins Regulated by the Algal Cell Cycle](#)

Share this paper:    

View more about this paper here: <https://typeset.io/papers/chloroplast-acquisition-without-the-gene-transfer-in-2axwmsafmi>

1 **Title**

2 Chloroplast acquisition without the gene transfer in kleptoplastic sea slugs, *Plakobranchus ocellatus*

3

4 **Authors**

5 Taro Maeda*¹, Shunichi Takahashi^{1,2}, Takao Yoshida³, Shigeru Shimamura³, Yoshihiro Takaki³, Yukiko Nagai³,

6 Atsushi Toyoda⁵, Yutaka Suzuki⁶, Asuka Arimoto⁷, Hisaki Ishii⁸, Noriyuki Satoh⁹, Tomoaki Nishiyama¹⁰,

7 Mitsuyasu Hasebe^{1,2}, Tadashi Maruyama¹¹, Jun Minagawa¹, Junichi Obokata⁸, Shuji Shigenobu*^{1,2}

8

9 **Affiliation**

10 1 National Institute for Basic Biology, Okazaki, Aichi, Japan

11 2 SOKENDAI, the Graduate University for Advanced Studies, Mishima, Shizuoka, Japan

12 3 Japan Agency for Marine-Earth Science and Technology, Yokosuka, Kanagawa, Japan

13 4 Tokai University, Hiratsuka, Kanagawa, Japan

14 5 National Institute of Genetics, Mishima, Shizuoka, Japan

15 6 The University of Tokyo, Bunkyo-ku, Tokyo, Japan

16 7 Marine Biological Laboratory, Hiroshima University, Onomichi, Hiroshima, Japan

17 8 Kyoto Prefectural University, Kyoto, Kyoto, Japan

18 9 Okinawa Institute of Science and Technology Graduate University, Okinawa, Japan

19 10 Advanced Science Research Center, Kanazawa University, Kanazawa, Japan

20 11 Kitasato University, Sagmihara, Kanagawa, Japan

21 ***Corresponding author**

22

23 **Email addresses:**

24 T. Maeda: maedat@nibb.ac.jp

25 ST: shun@nibb.ac.jp

26 TY: tyoshida@jamstec.go.jp

27 S. Shimamura: shimas@jamstec.go.jp
28 YT: takakiy@jamstec.go.jp
29 YN: nagai.y@jamstec.go.jp
30 AT: atoyoda@nig.ac.jp
31 YS: ysuzuki@k.u-tokyo.ac.jp
32 AA: aarimoto@hiroshima-u.ac.jp
33 KI: hsk.ishii@gmail.com
34 NS: norisky@oist.jp
35 TN: tomoakin@staff.kanazawa-u.ac.jp
36 MH: mhasebe@nibb.ac.jp
37 T. Maruyama: pee02660@nifty.ne.jp
38 JM: minagawa@nibb.ac.jp
39 JO: junichi.obokata@setsunan.ac.jp
40 S. Shigenobu: shige@nibb.ac.jp
41
42

43 **Abstract**

44 Some sea slugs sequester chloroplasts from algal food in their intestinal cells and photosynthesize for
45 months. This phenomenon, kleptoplasty, poses a question of how the chloroplast retains its activity without the
46 algal nucleus, and there have been debates on the horizontal transfer of algal genes to the animal nucleus. To
47 settle the arguments, we report the genome of a kleptoplastic sea slug *Plakobranthus ocellatus* and found no
48 evidence that photosynthetic genes are encoded on the nucleus. Nevertheless, we confirmed that photosynthesis
49 prolongs the life of mollusk under starvation. The data present a paradigm that a complex adaptive trait, as
50 typified by photosynthesis, can be transferred between eukaryotic kingdoms by a unique organelle transmission
51 without nuclear gene transfer. Our phylogenomic and transcriptomic analysis showed that genes for proteolysis
52 and immunity underwent gene expansion and are upregulated in the chloroplast-enriched tissue, suggesting that
53 these molluscan genes are involved in this DNA-independent transformation.

54 **Introduction**

55 Since the Hershey–Chase experiment (Hershey and Chase, 1952) which proved that DNA is the material
56 transferred to bacteria in phage infections, horizontal gene transfer (HGT) has been considered essential for
57 cross-species transformation (Arber, 2014). Although the prion hypothesis rekindled interest in proteins as an
58 element of phenotype propagation (Crick, 1970; Wickner et al., 2015), HGT is still assumed to be the cause of
59 transformation. For example, in secondary plastid acquisition scenario in dinoflagellates, 1) a non-phototrophic
60 eukaryote sequesters a unicellular archaeplastid; 2) endogenous gene transfer to the non-phototrophic eukaryote
61 leads to shrinkage of the archaeplastidan nuclear DNA (nucDNA); and 3) the archaeplastidan nucleus disappears
62 and its plastid becomes a secondary plastid in the host (Reyes-Prieto et al., 2007).

63 Chloroplast sequestration in sea slugs has attracted much attention due to the uniqueness of the phenotype
64 acquisition from algae. Some species of sacoglossan sea slugs (Mollusca: Gastropoda: Heterobranchia) can
65 photosynthesize using the chloroplasts of their algal food (Fig. 1) (de Vries and Archibald, 2018; Kawaguti,
66 1965; Pierce and Curtis, 2012; Rumpho et al., 2011; Serôdio et al., 2014). These sacoglossans ingest species-
67 specific algae and sequester the chloroplasts into their intestinal cells. This phenomenon is called kleptoplasty
68 (Gilyarov, 1983; Pelletreau et al., 2011). The sequestered chloroplasts (named kleptoplasts) retain their electron-
69 microscopic structure (Fan et al., 2014; Kawaguti, 1965; Martin et al., 2015; Pelletreau et al., 2011; Trench,
70 1969) and their photosynthetic activity (Cartaxana et al., 2017; Christa et al., 2014a; Cruz et al., 2015; Händeler
71 et al., 2009; Taylor, 1968; Teugels et al., 2008; Wägele and Johnsen, 2001; Yamamoto et al., 2009). The
72 retention period of the photosynthesis differs among sacoglossan species (one day to >300 days) (Christa et al.,
73 2015, 2014a, 2014b; Evertsen et al., 2007; Laetz and Wägele, 2017), development stages and depends on the
74 plastid “donor” species (Curtis et al., 2007; Laetz and Wägele, 2017).

75 The absence of algal nuclei in sacoglossan cells makes kleptoplasty distinct from other symbioses and
76 plastid acquisitions (de Vries and Archibald, 2018; Rauch et al., 2015). Electron microscopic studies have
77 indicated that the sea slug maintains photosynthetic activity without algal nuclei (Hirose, 2005; Kawaguti, 1965;
78 Laetz and Wägele, 2018; Martin et al., 2015; Pierce and Curtis, 2012). Because most photosynthetic proteins are
79 encoded on the algal nucleus rather than plastids, the mechanism by which photosynthetic proteins are
80 maintained in kleptoplasty is especially intriguing, given that the photosynthetic proteins have a high turnover

81 rate (de Vries and Archibald, 2018; Pelletreau et al., 2011). Previous PCR-based studies have suggested the
82 HGT of algal-nucleic photosynthetic genes (e.g., *psbO*) to the nucDNA of the sea slug *Elysia chlorotica* (Pierce
83 et al., 1996, 2010, 2007, 2003; Rumpho et al., 2008; Schwartz et al., 2014). A genomic study of *E. chlorotica*
84 (N50 = 824 bases) provided no reliable evidence of HGT but predicted that fragmented algal DNA and mRNAs
85 contribute to its kleptoplasty (Bhattacharya et al., 2013). Schwartz et al. (2014) reported *in situ* hybridization-
86 based evidence for HGT and argued that the previous *E. chlorotica* genome might overlook the algae-derived
87 gene. Although an improved genome of *E. chlorotica* (N50 = 442 kb) has published recently, no mention was
88 made of the presence or absence of algae-derived genes (Cai et al., 2019). The genomic studies of sea slug HGT
89 have been limited to *E. chlorotica*, and the studies have used multiple samples with different genetic
90 backgrounds for the genome assembling (Bhattacharya et al., 2013; Cai et al., 2019). The genetic diversity of
91 sequencing data may have inhibited genome assembling. Although transcriptome analyses of other sea slug
92 species failed to detect HGT (Chan et al., 2018; Wägele et al., 2011), the transcriptomic data was insufficient to
93 ascertain genomic gene composition (de Vries et al., 2015; Rauch et al., 2015).

94 Here, we present genome sequences of another sacoglossan species, *Plakobranthus ocellatus*, to clarify
95 whether HGT is the primary system underlying kleptoplasty. For over 70 years, *P. ocellatus* has been studied for
96 its ability to retain kleptoplasts for long-term (>3 months) (Christa et al., 2013; Evertsen et al., 2007; Greve et al.,
97 2017; Kawaguti, 1941; Trench et al., 1970; Wade and Sherwood, 2017; Wägele et al., 2011). However, recent
98 phylogenetic analysis showed *P. ocellatus* to be a species complex (set of closely related species) (Fig. 1) and,
99 therefore, useful to revisit previous studies about *P. ocellatus* (Christa et al., 2014c; Krug et al., 2013; Maeda et
100 al., 2012; Meyers-Muñoz et al., 2016; Yamamoto et al., 2013). Hence, we first confirmed the photosynthetic
101 activity and adaptive relevance of kleptoplasty to *P. ocellatus* type black (a species confirmed by Krug et al.
102 (2013) via molecular phylogenetics, hereafter “PoB”). We then constructed genome sequences of PoB (N50 =
103 1.45 Mb) and of a related species, *Elysia marginata* (N50 = 225 kb). By improving the DNA extraction method,
104 we have successfully assembled the genome sequences from a single sea slug individual in each species. Our
105 comparative genomic and transcriptomic analyses of these species demonstrate the complete lack of
106 photosynthetic genes in these sea slug genomes and provide evidence for an alternative hypothetical mechanism
107 of kleptoplasty.

108 **Results**

109 **Kleptoplast photosynthesis prolongs the life of *P. ocellatus* type black**

110 To explore the photosynthetic activity of PoB, we measured three photosynthetic indexes: the photochemical
111 efficiency of kleptoplast photosystem II (PSII), the oxygen production rate after starvation for 1-3 months, and
112 the effect of illumination on PoB longevity. The value of Fv/Fm, which reflects the maximum quantum yield of
113 PSII, was 0.68–0.69 in the “d38” PoB group (starved for 38 days), and was 0.57–0.64 in the “d109” group
114 (starved for 109–110 days). These values were only slightly lower than those of healthy *Halimeda borneensis*, a
115 kleptoplast donor of PoB, which showed Fv/Fm values of 0.73–0.76 (Fig. 2a, Supplementary Table 1),
116 indicating that PoB kleptoplasts retain a similar photochemical efficiency of PSII to that of the food algae for
117 over three months. On the measurement of oxygen concentrations in seawater, starved PoB (“d38” and “d109”)
118 displayed gross photosynthetic oxygen production (Fig. 2c). Without sea slugs, there was no light-dependent
119 increase in oxygen concentration: i.e., no detectable microalgal photosynthesis in the seawater (Supplementary
120 Fig. 1). The results demonstrate that PoB kleptoplasts retain photosynthetic activity for over three months.
121 consistent with previous *P. cf. ocellatus* studies (Christa et al., 2014c; Evertsen et al., 2007). We then measured
122 the longevity of starved PoB specimens under different light conditions. Mean longevity was 156 days under
123 continuous darkness and 195 days under a 12 h:12 h light-dark cycle ($p = 0.022$) (Fig. 2d, Supplementary Table
124 2), indicating that longevity was significantly extended when the animals were exposed to light. Our observation
125 is consistent with the observation of Yamamoto et al. (2013) that the survival rate of PoB after 21 days under
126 starvation is light-dependent. Although a study using *P. cf. ocellatus* reported that photosynthesis had no
127 positive effect on survival rate (Christa et al., 2014c), our results indicate that this finding is not applicable to
128 PoB. Taken together, the data for the three photosynthetic indexes indicate that kleptoplast photosynthesis
129 increases resistance to starvation in PoB.

130

131 **Photosynthetic genes in kleptoplasts**

132 To reveal the genetic autonomy of kleptoplasts, we sequenced whole kleptoplast DNAs (kpDNA) from PoB
133 and compared the sequences with algal plastid and nuclear genes. Illumina sequencing provided two types of
134 circular kpDNA and one whole mitochondrial DNA (mtDNA) (Fig. 3, Supplementary Fig. 2-7). The mtDNA

135 sequence was almost identical to the previously sequenced *P. cf. ocellatus* mtDNA (Greve et al., 2017)
136 (Supplementary Fig. 4). The sequenced kpDNAs corresponded with those of the predominant kleptoplast donors
137 of PoB (Maeda et al., 2012): i.e., *Rhipidosiphon lewmanomontiae* (AP014542, hereafter “kRhip”), and *Poropsis*
138 spp. (AP014543, hereafter “kPoro”) (Fig. 3b and Supplementary Fig. 5).

139 To determine if the kpDNA gene repertoires were similar to those of green algal chloroplast DNAs
140 (cpDNAs), we sequenced *H. borneensis* cpDNA and obtained 17 whole cpDNA sequences from public database
141 (Supplementary Fig. 6, and Supplementary Tables 3 and 4). The PoB kpDNAs contained all of the 59 conserved
142 chloroplastic genes in Bryopsidales algae (e.g., *psbA*, *rpoA*), although they lacked 4–5 of the dispensable genes
143 (i.e., *petL*, *psb30*, *rpl32*, *rpl12*, and *ccs1*) (Fig. 3c and Supplementary Fig. 7).

144 To test whether the kpDNAs contained no additional photosynthetic genes, we then used a dataset of 614
145 photosynthetic genes (hereafter, the “A614” dataset), which were selected from our algal transcriptome data and
146 public algal genome data (Supplementary Table 5 and 6). A tblastn homology search using the A614 obtained
147 no reliable hits (E-value <0.0001) against our kpDNA sequences, except for the gene *chlD*, which resembled
148 kpDNA-encoded *chlL* (Fig. 3de, Supplementary Figs. 8–10). A positive control search against an algal nucDNA
149 database (*C. lentillifera*, https://marinegenomics.oist.jp/umibudo/viewer/info?project_id=55) (Arimoto et al.,
150 2019) found reliable matches for 93% (575/614) of the queries (Fig. 3d), suggesting that the method has high
151 sensitivity. Thus, the comparison with algal plastid and nucleic genes clarified that the kpDNAs lack multiple
152 photosynthetic genes (e.g., *psbO*).

153

154 **Absence of horizontally transferred algal genes in the *P. ocellatus* type black nucleic genome**

155 To determine if the PoB nucleic genome contains algae-derived genes (i.e., evidence of HGT), we sequenced
156 the nuclear genome of PoB and searched for algae-like sequences in the gene models, genomic sequences, and
157 pre-assembled short reads. Our genome assembly contained 927.9 Mbp (99.1% of the estimated genome size,
158 8,647 scaffolds, N50 = 1.45 Mbp, 77,230 gene models) (INSD; PRJDB3267, Supplementary Figs. 11–14,
159 Supplementary Tables 7–10). BUSCO (Benchmarking Universal Single-Copy Orthologs) analysis using the
160 eukaryota_odb9 dataset showed high coverage (93%) of the eukaryote conserved gene set (Supplementary Table
161 7), indicating that our gene modeling was sufficiently complete to enable HGT searches.

162 Searches of the PoB gene models found no evidence of HGT from algae. Although simple homology
163 searches (blastp) against the RefSeq database found 127 PoB gene models with top-hits against Cyanobacteria
164 or eukaryotic algae, the prediction of taxonomical origin using multiple blast hit results (LCA analysis with
165 MEGAN software) (Huson et al., 2007) denied the algal-origin of the genes (Supplementary Table 11). A blastp
166 search using the A614 dataset which contains sequences of the potential gene donor (e.g., transcriptomic data of
167 *H. borneensis*) also determined no positive evidence of HGT (Supplementary Table 11).

168 In gene function assignment with gene ontology (GO) terms, no PoB gene model was annotated as a
169 “Photosynthesis (GO:0015979)”-related gene, although the same method found 72–253 photosynthesis-related
170 genes in the five algal species used as references (Fig. 4a). Our GO-analysis found six PoB genes assigned with
171 the child terms of “Plastid” (GO:0009536). However, ortholog search with animal and algal genes did not
172 support the algal origin of these genes (Supplementary Fig. 15 and 16; Supplementary Table 10). We consider
173 that these pseudo-positives in the similarity search and GO assignment are caused by sequence conservation of
174 the genes beyond the kingdom.

175 To confirm that our gene modeling did not overlook a photosynthetic gene, we directly searched the A614
176 dataset against the PoB and *C. lentillifera* (algal, positive control) genome sequences with tblastn and Exonerate
177 software (Slater and Birney, 2005). Against the *C. lentillifera* genome, we found 455 (tblastn) and 450
178 (Exonerate) hits; however, using the same parameters we only detected 1 (tblastn) and 2 (Exonerate) hits against
179 the PoB genome (Fig. 4b, Supplementary Fig. 17). The three loci detected in PoB contain the genes encoding
180 serine/threonine-protein kinase LATS1 (p258757c71.5), Deoxyribodipyrimidine photolyase (p855c67.9), and
181 phosphoglycerate kinase (p105c62.89). Phylogenetic analysis with homologous genes showed the monophyletic
182 relationships of these three genes with molluscan homologs (Supplementary Figs. 18–20). This indicates that the
183 three PoB loci contain molluscan genes rather than algae-derived ones. We thus conclude that our PoB genome
184 assembly contains no algae-derived photosynthetic genes.

185 To examine if our genome assembly failed to construct algae-derived regions in the PoB genome, we
186 searched for reads resembling photosynthetic genes among the pre-assembled Illumina data. From the 1,065
187 million pre-assembled reads, 1,698 reads showed similarity against 261 of the A614 dataset queries based on
188 MMseq2 searches. After normalization by query length, the number of matching reads against algal queries was
189 about 100 times lower than that against PoB single-copy genes: the normalized read count was 25 ± 105 (mean

190 \pm SD) for the A614 dataset and 2601 ± 2173 for the 905 PoB single-copy genes ($p < 0.0001$, Welch's two-
191 sample t -test) (Fig. 4c). This large difference indicates that many of the algae-like reads were derived from
192 contaminating microalgae rather than PoB nucDNA. Although, for five algal queries (e.g., peptidyl-prolyl cis-
193 trans isomerase gene), the number of matching reads was comparable between PoB and the A614 dataset (Fig.
194 4c), the presence of homologous genes on the PoB genome suggests that the reads were not derived from an
195 algae-derived region, but rather resemble molluscan genes. For example, simple alignment showed that the *C.*
196 *lentillifera*-derived g566.t1 gene, which encodes peptidyl-prolyl cis-trans isomerase, was partially similar to the
197 PoB p310c70.15 gene (Supplementary Fig. 21), and 76% (733/ 970) of reads that hit against g566.t1 were also
198 hitting against p310c70.15 under the same MMseq2 parameter (Supplementary Fig. 21). We hence consider that
199 no loss of algal-derived regions occurred in our assembly process.

200 Changing the focus to HGT of non-photosynthetic algal genes, we calculated the indexes for prokaryote-
201 derived HGT (h index) (Boschetti et al., 2012) and eukaryotic-algae-derived HGT (hA index, see Methods,
202 Supplementary Table 12) for PoB and two non-kleptoplastic gastropods (negative controls). We detected three
203 PoB gene models as potential algae-derived genes (Fig. 4d); however, two of these encoded a transposon-related
204 protein and the other encoded an ankyrin repeat protein that has a conserved sequence with an animal ortholog.
205 Furthermore, the non-kleptoplastic gastropods (e.g., *Aplysia californica*) had similar numbers of probable HGT
206 genes (Fig. 4d). Taking these results together, we conclude that there is no evidence of algae-derived HGT in
207 our PoB genomic data.

208 We then examined if algae-like RNA is present in PoB, because a previous study of another sea slug species
209 *E. chlorotica* hypothesized that algae-derived RNA contributes to kleptoplasty (Bhattacharya et al., 2013). This
210 previous study used short-read-based blast searches and RT-PCR analyses to detect algal mRNA (e.g., *psbO*
211 mRNA) in multiple adult *E. chlorotica* specimens (no tissue information was provided) (Bhattacharya et al.,
212 2013). To analyze the algal RNA distribution in PoB, we constructed 15 RNA-Seq libraries from six tissue types
213 (digestive gland [DG], parapodium, DG-exenterated parapodium [DeP], egg, head, and pericardium;
214 Supplementary Fig. 22) and conducted MMseq2 searches (Fig. 4c). Although almost all (594/614) of the A614
215 dataset queries matched no reads, 19 queries matched 1–10 reads, and the *C. lentillifera*-derived g566.t1 query
216 matched over 10 reads (Fig. 4e). This high hit rate for g566.t1 (Peptidyl-prolyl cis-trans isomerase in Fig. 4e),
217 however, is due to its high sequence similarity with PoB ortholog, p310c70.15 as mentioned above. A previous

218 anatomical study showed the kleptoplast density in various tissues to be DG > parapodium > DeP = head =
219 pericardium >>> egg (Hirose, 2005). Therefore, the amount of algae-like RNA reads did not correlate with the
220 kleptoplast richness among the tissues. Enrichment of algae-like RNA was only found in the egg. The PoB egg
221 is considered to be a kleptoplast-free stage and is covered by a mucous jelly, which potentially contains
222 environmental microorganisms (Fig. 4e and Supplementary Fig. 22c). We hence presume that these RNA
223 fragments are not derived from kleptoplasts but from contaminating microalgae. We conclude that our searches
224 for algae-like RNA in PoB found no credible evidence of algae-derived RNA transfer and no correlation
225 between algal RNA and kleptoplasty.

226

227 **Kleptoplasty-related *P. ocellatus* type black genes**

228 Because we found the PoB genome to be free of algae-derived genes, we considered that a neofunctionalized
229 molluscan gene might contribute to kleptoplasty. To find candidate kleptoplasty-related molluscan genes
230 (KRM), we focused on genes that were upregulated in DG (the primary kleptoplasty location) versus DeP in
231 the RNA-Seq data described above. We found 162 DG-upregulated genes (FDR <0.01, triplicate samples) (Fig.
232 5a and Supplementary Figs. 23–25). By conducting GO analysis, we identified the functions of 93 of the DG-
233 upregulated genes and showed that they are enriched for genes involved in proteolysis (GO terms: “Proteolysis”,
234 “Aspartic-type endopeptidase activity”, “Cysteine-type endopeptidase inhibitor activity”, and “Anatomical
235 structure development”), carbohydrate metabolism (“Carbohydrate metabolic process”, “One-carbon metabolic
236 process”, “Cation binding”, and “Regulation of pH”), and immunity (“Defense response”) (Supplementary
237 Table 13). Manual annotation identified the function of 42 of the remaining DG-upregulated genes. Many of
238 these are also related to proteolysis and immunity: three genes relate to proteolysis (i.e., genes encoding
239 interferon-gamma-inducible lysosomal thiol reductase, replicase polyprotein 1a, and phosphatidylethanolamine-
240 binding protein), and 21 genes contribute to natural immunity (i.e., genes encoding lectin, blood cell aggregation
241 factor, and MAC/Perforin domain-containing protein) (Supplementary Fig. 24 and 25). Our manual annotation
242 also found four genes encoding apolipoprotein D, which promotes resistance to oxidative stress (Charron et al.,
243 2008), and three genes involved in nutrition metabolism (i.e., genes encoding betaine–homocysteine S-
244 methyltransferase 1-like protein, intestinal fatty acid-binding protein, and cell surface hyaluronidase). Because

245 the analyzed slugs were starved for a month, we consider that the DG-upregulated genes contribute to
246 kleptoplasty rather than digestion.

247 We then conducted a comparative genomic analysis to find orthogroups that expand or contract in size along
248 the metazoan lineage to PoB. Our phylogenomic analysis showed that 6 of the 193 orthogroups that underwent
249 gene expansion in this lineage contained DG-upregulated genes, supporting the notion that these genes play a
250 role in kleptoplasty (Fig. 5b, Supplementary Figs. 26 and 27, Supplementary Table 14 and 15). The most
251 distinctive orthogroup was OG0000132, which contained 203 cathepsin D-like genes, 45 of which were DG-
252 upregulated, in PoB; Fisher's exact test supported the significant enrichment of the DG-upregulated genes (p
253 <0.0001 , Supplementary Table 15). Other heterobranchian mollusks only had 4–5 genes in OG0000132 (Fig. 5b
254 and Supplementary Fig. 28). These gene duplications in PoB might reduce selection pressure to maintain
255 function via redundancy, and promote new function acquirement of the paralogs, as occurs in the well-known
256 neofunctionalization scenario (Conrad and Antonarakis, 2007). DG-upregulated genes were also detected as
257 significantly enriched in OG0000005 (18 genes) and OG0000446 (4 genes) (both $p <0.0001$) (Fig. 5b), which
258 contain lectin-like and apolipoprotein D-like genes, respectively. DG-upregulated genes were detected in
259 OG0000002, OG0009179, and OG0000194, but were not significantly enriched in these orthogroups ($p > 0.05$).
260 OG0000002 contains the DG-upregulated gene for type 2 cystatin, but also contains various genes with reverse
261 transcriptase domains. This suggests that the reverse transcriptase domain clustered the various genes as one
262 orthogroup and the gene number expansion was due to the high self-duplication activity of the retrotransposon
263 in PoB. OG0009179 and OG0000194 contain DG-upregulated genes of unknown function. From the above
264 results, we finally selected 67 genes as promising targets of study for PoB kleptoplasty: 45 genes for cathepsin
265 D-like proteins, 18 genes for lectin-like proteins, and four genes for apolipoprotein D-like protein (gene
266 annotation data has been deposited in DOI 10.6084/m9.figshare.12318977).

267

268 **Evolution of the candidate KRMs**

269 For a more detailed analysis of the evolution of the kleptoplasty-related in sacoglossan lineages, we
270 constructed a new draft genome sequence of another sacoglossan sea slug *E. marginata* (previously identified as
271 *E. ornata* (Krug et al., 2013)). PoB and *E. marginata* belong to the same family (Plakobranchidae, Fig. 1e). Both
272 species sequester plastids from Bryopsidales algae; however, the kleptoplast retention time is limited to a few

273 days in *E. marginata* (Yamamoto et al., 2009). This suggests that their common ancestor obtained a mechanism
274 to sequester algal plastids, but *E. marginata* did not develop a system for their long-term retention. Hence, we
275 considered that comparing gene expansion in these species would clarify the genetic basis of plastid
276 sequestration and long-term retention.

277 Using the same methods as described for PoB, we sequenced one complete circular kpDNA, one complete
278 mtDNA, and 790.3 Mbp of nucDNA (87.8% of estimated genome size; 14,149 scaffolds; N50 = 0.23 Mbp;
279 70,752 genes, Supplementary Tables 7, 16, and 17) for *E. marginata*. The constructed gene models covered
280 89.5 % of the BUSCO eukaryota_odb9 gene set (Supplementary Table 7). No credible photosynthetic gene was
281 detected (annotation data, DOI 10.6084/m9.figshare.12318977).

282 We then phylogenetically analyzed the evolution of representative candidate PoB KRM (i.e., cathepsin D-
283 like, apolipoprotein D-like, and lectin-like genes). In the case of the cathepsin D-like genes, the sacoglossan
284 (PoB + *E. marginata*) genes formed a specific subgroup in the OG0000132-based phylogenetic tree (Fig. 5c, far
285 left), and the gene duplication in OG0000132 seemed to be accelerated along the PoB lineage (203 genes in PoB
286 versus 5 in *E. marginata*; Fig. 5b). All sacoglossan cathepsin D-like genes belonged to a clade with several other
287 heterobranchian homologs; this clade contained three sub-clades (α , β , γ in Fig. 5c). The basal α -clade contained
288 three *Aplysia californica* genes, one *Biomphalaria glabrata* gene, and three sacoglossan genes. The β - and γ -
289 clades contained sacoglossan genes only, and an *A. californica* gene was located at the basal position of the β -
290 and γ -clades. Almost all duplicated PoB genes (201/203) belonged to the γ -clade, which also included one *E.*
291 *marginata* gene (e8012c40.2). These phylogenetic relationships suggest that the γ -clade has undergone dozens
292 of gene duplication events in the PoB lineage. Interestingly, all DG-upregulated DEGs were contained in the γ -
293 clade, and the PoB paralogs belonging to the α - and β -clades showed different expression patterns from the γ -
294 clade paralogs; the gene p609c69.52 (α -clade) was ubiquitously expressed in the examined tissues, and
295 p374c67.53 (β -clade) was only expressed in the egg (Fig. 5c, center right). The mammalian genes encoding
296 cathepsin D and its analog (cathepsin E) are ubiquitously expressed on various tissue types (Benes et al., 2008).
297 We, therefore, consider that 1) the ubiquitously expressed p609c69.52 gene in α -clade is a functional ortholog of
298 the mammalian cathepsin D gene; 2) the p374c67.53 gene in β -clade relates sea slug embryo development; 3)
299 the γ -clade genes have been acquired with the development of plastid sequestration. The cathepsin D-like genes
300 formed multiple tandem repeat structures in the PoB genome, although other Heterobranchia had no tandem

301 repeat (Fig. 5c, far right; Supplementary Figs. 28 and 29). In *E. marginata*, the gene e8012c40.2 located at the
302 basal position of the γ -clade had no repeat structure, although two genes from the α -clade (e4981c37.5 and
303 e4981c37.4) and two from the β -clade (e2244c39.16 and e2244c39.20) made two tandem repeats
304 (Supplementary Figs. 28 and 29). The tree and repeat structure suggest that the γ -clade separated from the β -
305 clade as a single copy gene in the common ancestor of PoB and *E. marginata*, and duplicated in the PoB lineage
306 (Fig. 5c). The revealed genomic structure indicates that the duplicates were not due to whole-genome
307 duplication but rather a combination of several subgenomic duplication events: the dispersed duplicates are
308 likely due to replicative transposition by a transposable element, and the tandem repeats are likely due to a local
309 event (e.g., unequal crossover).

310 The gene duplication in OG0000446 seems to have happened in the PoB lineage and at the node between
311 PoB and *E. marginata* (Fig. 5b, Supplementary Figs. 30 and 31). The sacoglossan genes were duplicated in a
312 monophyletic clade (Clade I) only, and all DG-upregulated DEGs were contained in the Clade I. We
313 hypothesize that duplication on the common lineage relates to plastid sequestration, and the PoB-specific
314 duplication events contribute to long-term kleptoplasty. All DG-upregulated DEGs were contained in the Clade
315 I. We hypothesize that duplication on the common lineage relates to plastid sequestration, and the PoB-specific
316 duplication events contribute to long-term kleptoplasty.

317 In OG0000005 (lectin-like gene group), the gene counts were comparable between PoB (367) and *E.*
318 *marginata* (213) (Fig. 5b); however, the phylogenetic tree suggests that this similarity is due to different gene
319 duplication events in each species. One-by-one orthologous gene pairs were rare between PoB and *E. marginata*
320 (only 14 were detected), and many of the other homologs formed species-specific sub-clades (Supplementary
321 Fig. 32). Lectins are carbohydrate-binding molecules that mediate attachment of bacteria and viruses to their
322 intended targets (Lis and Sharon, 1998; Yamasaki et al., 2008). The observed gene expansions of lectin-like
323 genes in each of these sea slugs may widen their targets and may complicate the natural immune system to
324 distinguish the kleptoplast from other antigens. We detected four clades having expanded homologs on the
325 sacoglossan lineage (clades A–D in Supplementary Fig. 32). These clades contained all of the 34 DEGs between
326 DG and DeP tissues. The DG-upregulated and -downregulated genes were placed on different clades, except for
327 one DG-upregulated gene (p3334c67.98) in Clade A. These results indicate that the determined DEGs

328 duplicated after the specification of PoB, and the homologs have different expression patterns depending on the

329 clade.

330

331 Discussion

332 Here we demonstrate that 1) kleptoplast photosynthesis extends the lifetime of PoB under starvation, 2) the
333 PoB genome encodes no algal-nucleus-derived genes, and 3) PoB individuals upregulate genes for carbohydrate
334 metabolism, proteolysis and immune response in their digestive gland. Combination of the genomic and
335 transcriptomic analysis identified candidate KRM genes (apolipoprotein D-like, cathepsin D-like, and lectin-like
336 genes), which relates proteolysis and immune response. Together, the data present a paradigm of kleptoplasty in
337 which PoB obtains the adaptive photosynthesis trait by DNA-independent transformation.

338 Our genomic sequence of PoB clarified the gene repertory of its kpDNA, mtDNA, and nucDNA. The whole
339 kpDNA sequence indicated that PoB kleptoplasts can produce some proteins involved in photosynthesis (e.g.,
340 PsbA, a core protein in PSII) (Fig. 3) if gene expression machinery is sufficiently active, as reported in *E.*
341 *chlorotica* (Green et al., 2000; Pierce et al., 2007). We then demonstrated the absence of core photosynthetic
342 genes in PoB genome. For instance, we did not detect the genes encoding PsaF of photosystem I, PsbO of
343 photosystem II, or RbcS of Rubisco in kpDNAs, mtDNA, or nucDNA (Figs. 3 and 4), despite our queries (e.g.,
344 A612 dataset, Supplementary Table 6) containing multiple algal orthologs of these genes; these gene products
345 are essential for photosynthesis in various plants and algae, and are encoded on their nuclear genome, not plastid
346 genome (Farah et al., 1995; Izumi et al., 2012; Pigolev et al., 2009). This means that PoB can perform adaptive
347 photosynthesis (Fig. 2) without *de novo* synthesis of these gene products. The absence of algae-derived HGT is
348 consistent with previous transcriptomic analyses of *P. cf. ocellatus* (Wägele et al., 2011) and other sacoglossan
349 species (de Vries et al., 2015; Han et al., 2015; Wägele et al., 2011). A previous genome study of *E. chlorotica*
350 predicted that fragmented algal DNA and/or mRNAs contribute to its kleptoplasty (Bhattacharya et al., 2013),
351 and fluorescence *in situ* hybridization study detected algal gene signals on *E. chlorotica* chromosomes
352 (Schwartz et al., 2014). Although no photosynthesis-related algal genes were found in a more comprehensive
353 version of the *E. chlorotica* nuclear genome sequence, Cai et al. (2019) provided no discussion about the HGT.
354 From our results for PoB, we propose that algal DNA and/or RNA are not an absolute requirement for
355 kleptoplast photosynthesis.

356 Our combination of genomics and transcriptomics suggests that the maintenance of algae-derived protein
357 activity is the most probable mechanism for retaining PoB photosynthesis. Because of the limited longevity of

358 the photosynthetic proteins in algal cells and/or *in vitro* (Roberts et al., 2013), previous studies have discussed
359 elongation of algal protein lifespans via protective sea slug proteins as an alternative hypothesis to HGT (de
360 Vries and Archibald, 2018; Serôdio et al., 2014). Our study shows three types of molluscan genes as candidate
361 protective sea slug proteins: apolipoprotein D-like, cathepsin D-like, and lectin-like genes.

362 Previous RNA-Seq studies of *Elysia timida* and *E. chlorotica*, found upregulation of superoxide dismutase
363 (SOD) genes in response to photostress (Chan et al., 2018; de Vries et al., 2015), and postulated that SOD
364 protects algal proteins in the kleptoplasts from oxidative damage. We found no significant upregulation of the
365 SOD gene in PoB DG (Supplementary Fig. 24). However, we did find the upregulation of apolipoprotein D-like
366 genes and cathepsin D-like genes and the expansion of these genes in the PoB lineages (Fig. 5). Both proteins
367 are candidates for protective proteins against oxidative stress. Apolipoprotein D, a lipid antioxidant, confers
368 resistance to oxidative stress in higher plants and animal brain (Bishop et al., 2010; Charron et al., 2008).
369 Cathepsin D degrades intracellular proteins and contributes to the degradation of damaged mitochondria (Benes
370 et al., 2008). In general, damaged photosynthetic proteins generate abundant reactive oxygen species (ROS),
371 which promotes further protein damage. In PoB, the chain of protein inactivation may be broken through 1)
372 inhibition of ROS accumulation by apolipoprotein D-like proteins and 2) active degradation of damaged
373 proteins by cathepsin D-like proteases. Ortholog analysis of our new *E. chlorotica* data found no gene number
374 expansion of these homologs in *E. chlorotica*: i.e., only three apolipoprotein D-like homologs and four cathepsin
375 D-like homologs (Supplementary Table 18). Although the details of the retention process may differ among
376 species and abiotic conditions, it is attractive to speculate that oxidative stress resilience is of major importance
377 for kleptoplasty in multiple sacoglossan species.

378 The observed increase in expression of lectin genes in PoB DG tissue and their expansion in PoB lineages
379 (Fig. 5b, Supplementary Figs. 24 and 32) are also consistent with the kleptoplast photosynthetic protein
380 retention hypothesis. Almost all metazoans display natural immunity, and lectins are involved in
381 self-recognition in immunity (Geijtenbeek and Gringhuis, 2009; Worthley et al., 2005). The diverse lectins
382 expressed in PoB DG tissue may bind the antigens of algae-derived molecules, mediate detection of non-self-
383 proteins and/or saccharides, and lead to the selective degradation and retention of algae-derived proteins and
384 organelles.

385 Our genomic data indicate that proteomic analysis of kleptoplasts is warranted. A previous isotopic study
386 indicated that function-unknown sea slug proteins are transported to *E. chlorotica* kleptoplasts (Pierce et al.,
387 1996). Although several algal photosynthetic proteins have been immunoassayed in kleptoplasts, animal
388 nuclear-encoded proteins have not been examined (Green et al., 2000; Pierce et al., 1996). Our *in-silico* study
389 found no typical chloroplast localization signal in PoB KRM (Supplementary Figs. 28 and 30), however, our
390 genomic data will help the future identification of kleptoplast-localized sea-slug proteins by peptide mass
391 fingerprinting.

392 Here, we provide the first genomic evidence of photosynthesis acquisition without horizontal DNA or RNA
393 transfer. Previous studies have demonstrated that DNA is the core material for heredity (Hershey and Chase,
394 1952; Watson and Crick, 1953) and have assumed that horizontal DNA transfer causes cross-species phenotype
395 acquisition (Acuña et al., 2012; Anderson, 1970; Boto Luis, 2014; Dehal et al., 2002). Our studies, however,
396 indicate that PoB gains adaptive photosynthetic activity without acquiring any of the many algal-nucleic-genes
397 involved in photosynthesis. This is evidence that a phenotype (and organelle) can move beyond a species
398 without DNA or RNA transfer from the donor. Recent studies of shipworms (wood-feeding mollusks in the
399 family Teredinidae) showed that they utilize several symbiont-derived proteins for their food digestion
400 (O'Connor et al., 2014). Golden sweeper fish (*Parapriacanthus ransonneti*) gain the luciferase for their
401 bioluminescence from ostracod prey, suggesting phenotype acquisition via sequestration of a non-self-protein
402 (kleptoprotein) (Bessho-Uehara et al., 2020). These two examples of DNA/RNA-independent transformation,
403 however, are limited to the transfer of simple phenotypes that depend on just a few enzymes. In contrast, the
404 well-known complexity of photosynthesis suggests that sea slug kleptoplasty depends on DNA/RNA-
405 independent transformation of complex pathways requiring multiple enzymes (e.g., entire photosystems and the
406 Calvin-cycle). It is attractive to speculate that other symbiont-derived organelles (e.g., mitochondria), and
407 obligate endosymbiotic bacteria and protozoan kleptoplasts (e.g., in *Dinophysis acuminata*) (Hackett et al.,
408 2003) can move beyond the species via a DNA-independent system. Although several organisms have multiple
409 HGT-derived functional genes, it is still unclear how the organism evolutionary obtained the appropriate
410 expression control system of the non-self gene (Sasakura et al., 2016). Our PoB data suggest that the transfer of
411 adaptive complex phenotypes sometimes precede gene transfer from the donor species, having the potential to
412 explain the process of cross-species development of complex phenotypes. Some organisms may evolutionary

413 obtained the HGT-derived genes and appropriate control system of the gene expression after the transfer of
414 phenotype. Our finding of DNA-independent complex phenotype acquisition may open new viewpoints on
415 cross-species evolutionary interaction.

416

417

418 **#Materials and Methods**

419 **Sampling of sea slugs and algae**

420 Samples were collected from southwestern Japan; specifically, PoB and *H. borneensis* were collected at
421 shores of the island of Okinawa, and *E. marginata* was collected from Kinkowan bay. Regarding *B. hypnoides*, a
422 cultivated thallus was initially collected from Kinkowan bay and used in our laboratory for several years.
423 Collected samples of PoB and *E. marginata* in seawater were transported respectively to laboratories at NIBB
424 and Kyoto Prefectural University under dark conditions within 2 days. The samples were then acclimated in an
425 aquarium filled with artificial seawater (REI-SEA Marine II; Iwaki, Japan) at 24 °C.

426

427 **Photosynthetic activity of sea slugs and algae**

428 The photosynthetic activity of PoB was measured after 38, 109, or 110 days of incubation under a 12 h:12 h
429 light-dark cycle without food. During the light phase, the photosynthetic photon flux density was 10 μmol
430 photons $\text{m}^{-2} \text{s}^{-1}$ (LI-250A Light Meter with LI-193 Underwater Spherical Quantum Sensor, LI-COR). We did
431 not change the seawater during the incubation period except to adjust salinity using distilled water.
432 Photosynthetic activity indexes (oxygen generation rate and PAM Fluorometry) were measured using oxygen-
433 sensor spots (Witrox 4; Loligo Systems, Tjele, Denmark) and PAM-2500 (WALZ, Effeltrich, Germany,
434 Supplementary Fig. 1), respectively.

435 The oxygen-sensor spots were affixed to the inside of a glass respirometry chamber. Before performing
436 measurements, the system was calibrated using sodium sulfite (0% O_2 saturation) and fully O_2 -saturated
437 seawater (100% O_2 saturation). A sea slug was placed into a respirometry chamber filled with fully O_2 -saturated
438 filtered artificial seawater (7 ml). The top of the chamber was closed with a glass slide. All visible bubbles were
439 removed from the chamber. The chamber was maintained at a constant temperature (23-24 °C) using a water
440 jacket attached to temperature-controlled water flow. The Witrox temperature probe for calibration was
441 immersed in the water jacket.

442 The oxygen concentration was measured sequentially under changing light conditions. The percent O_2
443 saturation was monitored continuously and recorded using AutoResp software (Loligo Systems) for 10 min after
444 the respirometry chamber acclimation period (10 min). The oxygen consumption rate by respiration was

445 measured under the dark condition. Next, we exposed the respirometry chambers to the red LED light (800
446 $\mu\text{mol photons m}^{-2} \text{s}^{-1}$) to measure the change in the oxygen concentration under the light condition due to the
447 balance between the photosynthesis and respiration rates. The chambers were illuminated from the sides because
448 a top-mounted LED light increased the noise measured by the oxygen meter. The light direction with respect to
449 the sea slug was inconsistent because the slug continued to move around the chamber during the measurement
450 period. In sea slugs, the rate of photosynthesis appeared to be unaffected by the direction of illumination because
451 the rate of O_2 generation rate under a certain constant illumination did not change, regardless of the sea slug
452 position in the chamber. The percent O_2 saturation was measured for 10 min. One blank (i.e., without sea slug)
453 condition was run as a negative control to account for background biological activity in the seawater. AutoResp
454 software was used to convert the percent saturation to an oxygen concentration ($[\text{O}_2]$, $\text{mg O}_2 \text{ l}^{-1}$) based on the
455 rate of change in the percent O_2 saturation, the water temperature, and barometric pressure (fixed at 1013 Pa).
456 We performed a regression analysis by using the “lm” function in R (ver. 3.5.2, tidyverse 1.2.1 package) to
457 calculate the changing oxygen concentration rate under dark and light conditions, and obtained a gross oxygen
458 generation rate by photosynthesis ($\text{oL} + \text{oD} = \text{oG}$, oL ; Oxygen production rate under light, oD ; Oxygen
459 consumption rate under dark, oG ; gross oxygen generation by photosynthesis).

460 During the PAM Fluorometry analysis, each sea slug was caged in a single well of a 12-well cell culture
461 plate (Corning, Corning, NY, USA) after adaptation to the dark for 15 min. To ensure reproducibility, we caged
462 the sea slug upside down (i.e., the ventral surface was brought to the upside), softly squeezed the animal with a
463 plastic sponge, and connected the PAM light probe to the plate from underneath the well. Consequently, the
464 samples could not move during the measurement, and the PAM light probe always measured the fluorescence of
465 the dorsal surface. The maximal quantum yield, F_v/F_m , was determined by a saturation pulse of $>8000 \mu\text{mol}$
466 $\text{photons m}^{-2} \text{s}^{-1}$ and a measurement light of $0.2 \mu\text{mol photons m}^{-2} \text{s}^{-1}$.

467

468 **Effect of the light condition on *P. ocellatus* longevity**

469 We measured the longevity of PoB using a modified medaka (Japanese rice fish) housing rack system (Iwaki,
470 Japan). For the longevity measurement, we used different individuals from the photosynthetic activity
471 measurement. The longevity was investigated from the samples used in the above-mentioned photosynthetic

472 activity measurement. Using centrally filtered systems, our water tank rack maintained consistent water
473 conditions (e.g., temperature and mineral concentration) among the incubation chambers (sub-tanks) and
474 enabled a focus on the effect of the light condition. After acclimating the collected sea slugs under the same
475 conditions for 1 week in an aquarium, the organisms were incubated separately for 8 months under different
476 light conditions (continuous dark and 12 h:12 h light-dark cycle). We evaluated the conditions of the sea slugs
477 daily and defined death as a sea slug that remained motionless for 30 seconds after stimulation (i.e., touching
478 with plastic bar).

479

480 **Sequencing of *H. borneensis* chloroplast DNA**

481 We used a combination of pyrosequencing and Sanger sequencing to evaluate *H. borneensis* cpDNA.
482 Collected *H. borneensis* thalli were washed with tap water to remove the attached organisms. The cleaned thalli
483 (27 g) were frozen in liquid nitrogen, ground with a T-10 Basic Homogenizer (IKA, Germany) to a fine powder,
484 suspended in 15 mL of AP1 buffer from a DNeasy Plant Mini Kit (Qiagen, Hilden, Germany), and centrifuged
485 (500 × g, 1 min) to remove the calcareous parts. Total DNA was purified from the supernatant according to the
486 protocol supplied with the DNeasy Plant Mini Kit. The resulting DNA yield (76.8 µg) was measured using a
487 dsDNA HS Assay Qubit Starter Kit (Thermo, Waltham, MA, USA), and was used to prepare a single-fragment
488 library for pyrosequencing. The Pyrosequencer GS-FLX Titanium platform (Roche, Germany) was used to
489 generate 23.04 Mb of total singleton reads (68,032 reads, average read length: 368 bp). After filtering low-
490 quality reads, the remaining 21,865 reads (~8 Mb) were submitted for assembly by Newbler (Roche). Of the
491 6,309 obtained contigs (N50 = 663 bp), the cpDNA sequences were identified by blastx searches (ver. 2.2.28)
492 against the protein-coding sequences of cpDNA from the chlorophyte alga *B. hypnoides* (NC_013359). The gaps
493 between the four identified contigs (55,551, 21,264, 8,076, and 3,435 bp) and ambiguous sites in the contigs
494 were amplified by PCR using inverse primers. PCR products were sequenced by primer walking and Sanger
495 sequencing with Takara LA Taq (Takara, Japan), a dGTP BigDye Terminator Cycle Sequencing FS Ready
496 Reaction Kit (Thermo), and an ABI PRISM 3130xl DNA Sequencer (Thermo). Regions that could not be read
497 by direct sequencing were amplified using specific primers, cloned with a TOPO TA cloning kit (Thermo), and
498 sequenced with plasmid-specific primers. Complete cpDNA sequences were obtained by assembling the GS-
499 FLX contigs and reads generated by Sanger sequencing using Sequencher ver. 4.10 (Gene Codes Corporation,

500 MI, USA). All open reading frames >100 bp were annotated using a blastx search (ver. 2.2.31+) against the non-
501 redundant protein sequences (nr) database in GenBank and a tblastx search of chloroplast genes from other algae
502 (*B. hypnoides*, *Chlamydomonas reinhardtii*, *V. litorea*, and *H. borneensis*). Introns were detected using
503 RNAweasel (Gautheret and Lambert, 2001), Rfam (Kalvari et al., 2018), and Mfold (Zuker, 2003). We
504 confirmed the splicing sites via alignment with orthologous genes from other green algal cpDNAs. We used
505 MAFFT v7.127b (Kato and Standley, 2013) to perform the alignment. The origins of bacteria-like proteins
506 were explored using a blastx search against the nr database and a phylogenetic analysis with blast-hit sequences.
507 We used MAFFT (Kato and Standley, 2013) for alignment, Trimal v1.4 (Capella-Gutiérrez et al., 2009) for
508 trimming, and RaxML v8.2.4 (Stamatakis, 2014) for phylogenetic tree construction. The resulting gene maps
509 were visualized using Circos ver. 0.69-2.

510 **Sequencing of kpDNAs from *P. ocellatus***

511 Kleptoplast sequences were generated using an Illumina system. Total DNA was extracted from the
512 digestive gland (kleptoplast-rich tissue) and parapodia (including the digestive gland, kleptoplast-less muscle,
513 and reproductive systems) of a single PoB individual using a CTAB-based method (Murray and Thompson,
514 1980). Two Illumina libraries with 180- and 500-bp insertions were constructed from each DNA pool
515 (DRR063261, DRR063262, DRR063263, and DRR063264). An S220 Focused-Ultrasonicator (Covaris, MA,
516 USA), Pippin Prep (Sage Science, MA, USA), and a TruSeq DNA Sample Prep Kit (Illumina, CA, USA) were
517 used for DNA fragmentation, size selection, and library construction, respectively. Libraries were sequenced
518 (101 bp from each end) on a HiSeq 2500 platform (Illumina). A total of 42,206,037 raw reads (8.53 Gb) were
519 obtained. After filtering the low-quality and adapter sequences, the remaining 5.21 Gb of sequences were used
520 for assembly. Paired sequences from 180-bp libraries were combined into overlapping extended contigs using
521 FLASH ver. 1.2.9 (Magoc and Salzberg, 2011) with the default settings. An input of 14,867,401 paired-end
522 sequences and FLASH were used to construct 13,627,554 contigs (101–192 bp). The joined fragments and
523 filtered paired sequences from 500-bp libraries were assembled using Velvet assembler ver. 1.2.07 (Zerbino and
524 Birney, 2008) with parameters that were optimized based on the nucDNA and kpDNA sequence coverage
525 depths; the estimated nucDNA depth was approximately 30× based on the k-mer analysis, and the predicted
526 kpDNA depth was 272× based on the read mapping to previously obtained kleptoplast *rbcl* sequences
527 (AB619313; 1195 bp) using Bowtie2 ver. 2.0.0 (Langmead and Salzberg, 2012). After several tests to tune the

528 Velvet parameters, the best assembly was achieved with a k-mer of 83 and exp_cov of 50. The resulting
529 assembly comprised 1,537 scaffolds (>2000 bp) containing 4,743,113 bp (N50 = 2830 bp). We then identified
530 two kpDNAs (AP014542 and AP014543) from this assembly based on the sequence similarity with *H.*
531 *borneensis* cpDNA and a mapping back analysis. blastx ver. 2.2.31 assigned bit scores >1000 to the two
532 scaffolds (AP014542 = 1382, AP014543 = 1373, database = coding sequences in the obtained *H. borneensis*
533 cpDNA, query = all constructed scaffolds). Mapping back, which was performed using BWA ver. 0.7.15-r1140,
534 showed that the coverage depths of AP014542 and AP014543 correlated with the relative abundance of
535 kleptoplasts; the average coverage depth of the read was increased by 2–4 fold in a library from kleptoplast-rich
536 tissue (DRR063263) relative to a library from kleptoplast-poor tissue (DRR063261). The same degree of change
537 was never observed in other scaffolds (Supplementary Fig. 33).

538 The two kleptoplast sequences were annotated and visualized using the same method described for *H.*
539 *borneensis* cpDNA. The phylogenetic positions of PoB kleptoplasts and algal chloroplasts were analyzed using
540 the *rbcL* gene sequences from 114 ulvophycean green algae according to the maximum likelihood method (Fig.
541 3b, Supplementary Fig. 5). A phylogenetic tree was constructed according to the same method used to search for
542 the origins of bacteria-like genes in *H. borneensis* cpDNA.

543

544 **Analysis of the *H. borneensis* and *B. hypnoides* transcriptomes**

545 De novo transcript profiles of *H. borneensis* and *B. hypnoides* were obtained from Illumina RNA-seq data.
546 We extracted total RNA using the RNeasy Plant Mini Kit (Qiagen), constructed single Illumina libraries using
547 the TruSeq RNA Sample Prep Kit, and sequenced the library of each species (101 bp from each end) on a HiSeq
548 2500 platform. A total of 290,523,622 reads (29 Gb) and 182,455,350 raw reads (18 Gb) were obtained for *H.*
549 *borneensis* and *B. hypnoides*, respectively. After filtering the low-quality and adapter sequences, the obtained
550 reads were assembled using Trinity ver. 2.4.0 (Grabherr et al., 2011) and clustered using CD-Hit ver. 4.6 (Fu et
551 al., 2012) with the -c 0.95 option. The TransDecoder ver. 2.0.1 was used to identify 26,652 and 24,127 candidate
552 coding regions from *H. borneensis* and *B. hypnoides*, respectively. The gene completeness of the transcripts was
553 estimated using BUSCO ver. 2.0 (Waterhouse et al., 2018). The obtained *H. borneensis* transcripts covered
554 86.5% (262/303) of the total BUSCO groups), while the *B. hypnoides* transcripts covered 92.7% (281/303) of
555 the conserved genes in Eukaryota (database, eukaryota_odb9). The transcripts were annotated using AHRD ver.

556 3.3.3 (<https://github.com/groupschoof/AHRD>) based on the results of a blastp search against nr, RefSeq, and
557 *Chlamydomonas* proteome dataset on UniProt. The composed functional domains on the transcripts were
558 annotated using InterProScan ver. 5.23-62 (Jones et al., 2014). To distinguish the reliable target species
559 transcripts, we predicted the original transcript species using MEGAN ver. 5 (Huson et al., 2007) and selected
560 11,629 and 8,630 transcripts as viridiplantal genes. We have presented the details of the annotation procedure
561 visually in Supplementary Figs. 8 and 9.

562 We manually selected a query dataset from the algal transcripts to search algae-derived genes on the sea
563 slug DNAs. We selected 176 and 129 transcripts from *H. borneensis* and *B. hypnoides*, respectively. To perform
564 more comprehensive searches, we also obtained queries from three public genomic datasets derived from
565 *Caulerpa lentillifera*, *Chlamydomonas reinhardtii*, and *Cyanidioschyzon merolae*; these queries were termed the
566 A614 dataset (Supplementary Table 6, DOI 10.6084/m9.figshare.12318947).

567

568 **Sequencing of the *P. ocellatus* type black genome**

569 The mean nucDNA size in three PoB individuals was estimated using flow cytometry. Dissected
570 parapodial tissue (5 mm²) was homogenized in 1 ml of PBS buffer containing 0.1 % triton X-100 (Thermo) and
571 0.1 % RNase A (Qiagen) using a BioMasher (Nippi, Tokyo, Japan). We then filtered the homogenate through a
572 30-µm CellTrics filter (Sysmex, Hyogo, Japan) and diluted the filtrate with PBS buffer to a density of <5×10⁶
573 cell/ml. The resulting solution was mixed with genome size standard samples and stained with a 2% propidium
574 iodide solution (SONY, Tokyo, Japan). We used *Acyrtosiphon pisum* (genome size = 517 Mb) and *Drosophila*
575 *melanogaster* (165 Mbp) samples processed using the same method described for PoB as genome size standards.
576 The mixture was analyzed on a Cell Sorter SH800 (SONY) according to the manufacturer's instructions. We
577 repeated the above procedure for three PoB individuals and determined an estimated genome size of 936 Mb
578 (Supplementary Fig. 12).

579 Genomic DNA was extracted from a single PoB individual using the CTAB-based method (Murray and
580 Thompson, 1980). The adapted buffer compositions are summarized in Supplementary Table 19. A fresh PoB
581 sample (collected on October 17, 2013, and starved for 21 days) was cut into pieces and homogenized in
582 2×CTAB buffer using a BioMasher. To digest the tissues, we added a 2% volume of Proteinase K solution
583 (Qiagen) and incubated the sample overnight at 55° C. The lysate was emulsified by gentle inversion with an

584 equal volume of chloroform; after centrifugation (12,000× g, 2 min), the aqueous phase was collected using a
585 pipette. This phase was combined with a one-tenth volume of 10% CTAB buffer, mixed well at 60 °C for 1 min,
586 and again emulsified with chloroform. These 10% CTAB buffer and chloroform treatment steps were repeated
587 until a clear aqueous phase was achieved. We then transferred the aqueous phase to a new vessel, overlaid an
588 equal volume of CTAB precipitation buffer, and mixed the liquids gently by tapping. The resulting filamentous
589 precipitations (DNA) were removed using a pipette chip and incubated at room temperature for 10 min in High
590 Salt TE buffer. We then purified the DNA according to the protocol supplied with the DNeasy Blood and Tissue
591 Kit (Qiagen); briefly, we transferred the supernatant after vortex mixing, added equal volumes of buffer AL
592 (supplied with the kit) and EtOH to the supernatant, and processed the sample on a Qiagen spin column
593 according to the protocol. We obtained a final DNA quantity of 15 µg from a PoB individual.

594 The genomic sequence of PoB was obtained via Illumina paired-end and mate-pair DNA sequencing.
595 Two paired-end Illumina libraries containing 250- and 600-bp insertions (DRR029525, DRR029526) were
596 constructed using a TruSeq DNA Sample Prep Kit (Illumina). Three mate-pair libraries with 3k-, 5k-, and 10k-
597 bp insertions (DRR029528, DRR029529, DRR029530) were constructed using a Nextera Mate Pair Library
598 Prep Kit (Illumina). The libraries were sequenced (150 bps from each end) on a HiSeq 2500 platform (Illumina).
599 A total of 1,130,791,572 and 787,040,878 raw reads were obtained for the paired-end (170 Gb) and mate-pair
600 (118 Gb) libraries, respectively. After filtering the low-quality and adapter sequences, the remaining 161 Gb of
601 sequences were assembled using Platanus assembler ver. 1.2.1 (Kajitani et al., 2014) with the default setting.
602 The assembly comprised 8,716 scaffolds containing 928,345,517 bp. Repetitive regions were masked using a
603 combination of RepeatModeler ver. open-1.0.8 and RepeatMasker ver. open-4.0.5
604 (<http://www.repeatmasker.org>). We used the default parameters for identification and masking. A total of
605 268,300,626 bp (29%) of the assemblies were masked with RepeatMasker.

606 We used strand-specific RNA-Seq sequencing for gene modeling. PoB RNA was extracted from an
607 individual after starvation for 20 days (collected on October 17, 2013). We used TRIzol™ Plus RNA
608 Purification Kit (Thermo) to extract RNA according to the manufacturer's protocol. A paired-end Illumina
609 library (DRR029460) was constructed using the TruSeq Stranded mRNA LT Sample Prep Kit (Illumina).
610 Libraries were sequenced (150 bp from each end) on a HiSeq 2500 platform (Illumina). The library produced a
611 total of 286,819,502 raw reads (28 Gb).

612 The PoB assemblies were processed using single transcript-based gene model construction pipeline
613 (AUGUSTUS ver. 3.2) (Stanke and Morgenstern, 2005), two transcriptomic data mapping tools (Trinity ver.
614 2.4.0 and Exonerate ver. 2.2.0) (Grabherr et al., 2011; Slater and Birney, 2005), and two non-transcript-based
615 model construction pipelines (GeneMark-ES ver. 4.33 and glimmerHMM ver. 3.0.4) (Majoros et al., 2004; Ter-
616 Hovhannisyan et al., 2008). The four obtained gene sets were merged with the EVidenceModeler ver. 1.1.1
617 pipeline (Haas et al., 2008) to yield a final gene model set. For AUGUSTUS, we used Braker pipeline ver. 1.9
618 (Hoff et al., 2019) to construct PoB-specific probabilistic models of the gene structure based on strand-specific
619 RNA-Seq data. After filtering the low-quality and adapter sequences, the remaining 181,873,770 RNA-Seq
620 reads (16 Gb) were mapped to the PoB genome assembly using TopHat ver. v2.1.1 (Kim et al., 2013) with the
621 default setting, as well as to the Braker pipeline-constructed PoB-specific probabilistic models from mapped
622 read data. TopHat mapped 132,786,439 of the reads (73%) to the PoB model. AUGUSTUS then predicted
623 78,894 gene models from the TopHat mapping data (as splicing junction data) and the Braker probabilistic
624 model. Using Trinity and Exonerate, we then constructed de novo transcriptomic data from the RNA-Seq data
625 and aligned these to the genome. Trinity constructed 254,336 transcripts, which were clustered to 194,000
626 sequences using CD-Hit ver. 4.6 (-c 0.95); subsequently, Transdecoder identified 44,596 protein-coding regions
627 from these sequences. Exonerate (--bestn 1 --percent 90 options) then aligned the 13,141 of the transcripts to the
628 genome. GeneMark-ES with the default setting predicted 107,735 gene models, and glimmerHMM predicted
629 115,633 models after the model training, with 320 manually constructed gene models from long scaffolds.
630 EVidenceModeler was then used to merge the model with the following weight settings: AUGUSTUS = 9,
631 Exonerate = 10, GeneMark-ES = 1, glimmerHMM = 2. Finally, EVidenceModeler predicted 77,444 gene
632 models.

633 We then removed the contaminant-derived bacterial scaffolds from the PoB assemblies. We defined
634 bacterial scaffolds as those encoding >1 bacterial gene with no lophotrochozoan gene. The bacterial genes were
635 predicted using MEGAN software according to a blastp search against the RefSeq database. Of the 40,330 gene
636 hits identified from the RefSeq data, MEGAN assigned the origins for 39,113 genes. Specifically, 719 and
637 23,559 genes were assigned as bacterial and lophotrochozoan genes, respectively. Fifty-five of the 8,716
638 scaffolds contained two or more bacterial genes and no lophotrochozoan gene and were removed
639 (Supplementary Table 8).

640 We also removed kleptoplast- or mitochondria-derived scaffolds from the assemblies (Supplementary
641 Table 9). We determined the source of scaffolds based on blast bit score against the three referential
642 organelle DNAs (kRhip AP014542, kPoro AP014543, and PoB mtDNA AP014544) and the difference of
643 the read depth value from the other (nuclear-derived) scaffolds. Our blastn search detected 13 and one
644 scaffolds as sequences of kleptoplast or mitochondrial origin, respectively (bit score >1000, Supplementary
645 Table 9). Mapping back of the Illumina read (DRR029525) by Bowtie ver. 2.4.1 indicated that the depth
646 values of the 14 scaffolds were 537- 5143, and the averaged depth value of the other scaffolds was 31
647 (Supplementary Tables 8 and 9), indicating the 14 scaffolds are derived from organelle DNAs or repetitive
648 region on the nuclear DNA. Mapping of the reads derived from DG (kleptoplast enriched tissue)
649 (DRR063263) and parapodium (including a muscle, gonad, and digestive gland) (DRR063261) indicated
650 that the relative read depth of the 13 kpDNA-like scaffolds (against the averaged depth value of other
651 scaffolds) was higher in the DG sample than in the parapodium sample, supporting that the sequences are
652 derived from the kleptoplast (Supplementary Fig. 34). We then confirmed the scaffolds contain no algal-
653 nuclear-derived photosynthetic gene using two methods; dot-plots with referential organelle DNAs and
654 homology search using A612 query set (Supplementary Fig. 17, 35-37). Hence, even if the scaffolds
655 originate from the nucleus, our results indicate no evidence of HGT of photosynthetic algal nuclear-
656 encoded genes. We deposited the removed scaffolds sequences in the FigShare under DOI
657 10.6084/m9.figshare.12587954.

658 The final PoB assembly comprised 8,647 scaffolds containing 927,888,823 bp (N50 = 1,453,842 bp) and
659 77,230 genes. Gene completeness was estimated using BUSCO ver. 2.0 (Waterhouse et al., 2018). The predicted
660 gene models were annotated using AHRD ver. 3.3.3. The results of a blastp search against the SwissProt,
661 Trembl, and *Aplysia californica* proteome datasets on UniProt were used as reference data for AHRD under the
662 following weight parameter settings: SwissProt = 653, Trembl = 904, and *A. californica* = 854. The functional
663 domains were annotated using InterProScan ver. 5.23-62.

664 We performed a blastp analysis against the RefSeq database to identify algae-derived genes from the
665 constructed genes models. After translating the protein-encoding region to amino acid sequence data, we
666 adapted the blastp search to include the “-e-value 0.0001” option. The output was analyzed using MEGAN

667 software with the following LCA and analysis parameters: Min Score = 50, Max Expected = 1.0E-4, Top
668 Percent = 20, Min Support Percent = 0.1, Min Support = 1, LCA percent = 90, and Min Complexity = 0.3.

669 The GO annotation was assigned using Blast2GO ver. 5.2.5 according to the blastp searches against the
670 RefSeq database and InterProScan results. We then used SonicParanoid ver. 1.0.11 for orthogroup detection.
671 The species analyzed in the orthogroup detections are summarized in Supplementary Table 10. The phylogenetic
672 tree was constructed using IQ-tree. The resulting trees were visualized using iTol ver. 4.

673 We used Exonerate ver. 2.2.0 (with the --bestn 1 --model protein2genom options) to identify algal genes
674 in the PoB genome. We used the A614 dataset as a query after translating the sequence to amino acids. *Caulerpa*
675 *lentillifera* (green algae) genomic data were used as a control to estimate the sensitivity of our method. The
676 results were handled and visualized using R (tidyverse packages ver. 1.2.1).

677 We used MMseq2 ver. 2.6 (--orf-start-mode 1) to search for algae-like reads among the trimmed Illumina
678 reads. The matching threshold was set using a default E-value <0.001. As a positive control, we selected PoB
679 genes from the BUSCO analysis of our genomic model data. We selected 911 gene models detected by BUSCO
680 ver. 2 as single-copy orthologs of the metazoa_odb9 gene set and named the dataset P911 (DOI
681 10.6084/m9.figshare.12318977).

682 The horizontal gene transfer index “h” and the modified index “hA” were calculated using our R script,
683 HGT_index_cal.R (https://github.com/maedat/HGT_index_cal; R ver. 3.6.1). The “h” index was calculated as
684 the difference in bit scores between the best prokaryote and best eukaryote matches in the blast alignments, and
685 “hA” was calculated as the difference in bit scores between the best lophotrochozoan and best algae matches.
686 The blast databases of adapted species are summarized in Supplementary Table 12.

687

688 **RNA-Seq analysis of *P. ocellatus* type black tissues**

689 Total RNA samples from five PoB individuals and one egg mass were obtained for a gene expression
690 analysis. An overview of sample preparation is illustrated in Supplementary Fig. 22. Collected adult PoB
691 individuals were dissected manually after an incubation of 21–94 days. An egg mass was obtained via
692 spontaneous egg lying in an aquarium. We used a TRIzol™ Plus RNA Purification Kit (Thermo) to extract
693 RNA according to the manufacturer’s protocol. We constructed six paired-end and nine single-end Illumina
694 libraries using a combination of the RiboMinus Eukaryote Kit (Thermo), RiboMinus concentration module

695 (Thermo), and TruSeq RNA Sample Preparation Kit v2 (Illumina) according to the manufacturers' protocols.
696 Libraries were sequenced (101 bp) on a HiSeq 2500 platform (Illumina). A total of 280,445,422 raw reads (28
697 Gb) were obtained from the libraries (DOI 10.6084/m9.figshare.12301277).

698 After filtering the low-quality and adapter sequences, 150,701,605 RNA-Seq reads (13 Gb) were obtained.
699 We used only the R1 reads for the six paired-end datasets. We used MMseq2 to identify algae-derived reads
700 from the trimmed reads, using the A614 dataset as a query. We applied the same parameters as the above-
701 described DNA read search. The PoB gene dataset P911 was also used as a positive control.

702 We used the Hisat-stringtie-DESeq2 pipeline to conduct a differential gene expression analysis of DGs
703 and DG-exenterated parapodia (epidermis, muscle, and reproductive systems, Dep). According to the Stringtie
704 protocol manual (<http://ccb.jhu.edu/software/stringtie/index.shtml?t=manual>), trimmed RNA-Seq reads were
705 mapped to the PoB genome assembly using Hisat2 ver. 2.1.0 with the default setting. The obtained BAM files
706 were processed using Stringtie ver. 1.3.4d (-e option) with PoB gene model data (gff3 format) acquired through
707 the above-mentioned EvidenceModeler analysis. The resulting count data were analyzed using R and the
708 DESeq2 package, and 1,490 differentially expressed genes (p-value <0.01 and padj <0.05) were identified
709 between the tissues. We used the GSeq (Young et al., 2010) and topGO packages in R to apply a GO
710 enrichment analysis to the upregulated genes in DG tissue (threshold: p-value <0.01).

711

712 **Sequencing of the *E. marginata* genome**

713 The *E. marginata* genome sequencing process was nearly identical to the methodology applied to PoB.
714 Flow cytometry yielded an estimated genome size of 900 Mb. We extracted genomic DNA from an individual
715 using a CTAB-based method. We constructed four types of Illumina libraries: two paired-end libraries with 250-
716 and 500-bp insertions, and two mate-pair libraries with 3k- and 5k-bp insertions (DOI
717 10.6084/m9.figshare.12301277). Using the HiSeq 2500 platform (Illumina), we obtained 562,732,268 and
718 608,977,154 raw reads for the paired-end (84 Gb) and mate-pair (91 Gb) libraries, respectively. After filtering
719 the low-quality and adapter sequences, the remaining 40 Gb of sequences were assembled using the Platanus
720 assembler. The assembly comprised 14,285 scaffolds containing 791,005,940 bp.

721 For gene modeling, strand-specific RNA-Seq sequencing of *E. marginata* was performed. A paired-end
722 Illumina library (DRR029460, also see DOI 10.6084/m9.figshare.12301277) was constructed using a TruSeq

723 Stranded mRNA LT Sample Prep Kit (Illumina) and an RNA sample extracted from an *E. marginata* individual
724 via a TRIzol™ Plus RNA Purification Kit (Thermo). Libraries were sequenced (150 bp from each end) on a
725 HiSeq 2500 platform (Illumina). A total of 286,819,502 raw reads (28 Gb) were obtained from the library. Using
726 the gene modeling procedure described for PoB, EVIDENCEModeler constructed 71,137 gene models of the
727 genomic assemblies based on the RNA-Seq data.

728 We next removed the contaminant-derived bacterial scaffolds from the genomic assemblies. Using the
729 same gene annotation as applied to PoB, we determined that the 110 of the 14,285 scaffolds contained >1
730 bacterial genes and no lophotrochozoan gene and removed these scaffolds. The organelle-derived scaffolds
731 (kleptoplast DNA and mitochondrial DNA) were identified using blastn searches and removed from the final
732 assemblies. A blastn search (query = all scaffolds, database = chloroplast DNA of *B. hypnoides* NC_013359.1 or
733 mitochondrial DNA of PoB) identified 25 kleptoplast-matching and one mitochondria-matching scaffold (bit
734 score >1000). We then reassembled the complete kleptoplast DNA and mitochondrial DNA using the same
735 method as described for PoB organellar DNA assembling.

736 **Ortholog analysis of sacoglossan genes**

737 Orthologous relationships were classified using OrthoFinder (ver. 2.2.3) (Emms and Kelly, 2015), and
738 rapidly expanded/contracted families identified from the OrthoFinder results were analyzed using CAFE (ver.
739 4.2) (Han et al., 2013). CAFE analysis used 16 metazoan species as reference species (Supplementary Fig. 23).
740 Phylogenetic trees for CAFE were constructed using PREQUAL (ver. 1.02) (Whelan et al., 2018) for sequence
741 trimming, MAFFT (ver. 7.407) for sequence alignment, IQ-tree (ver. 1.6.1) for the maximum likelihood (ML)
742 analysis, and r8s (v1.81) (Sanderson, 2003) for conversion to an ultrametric tree. An ML tree was constructed
743 from 30 single-copy genes in 15 major species according to the OrthoFinder results (DOI
744 10.6084/m9.figshare.12319862), and was converted to an ultrametric tree based on the divergence times of
745 Amphiesmenoptera-Antliophora (290 Myr) and Euarchontia-Glires (65 Myr).

746 We also analyzed the expanded/contracted families using the Z-scores of the assigned gene numbers for
747 each orthogroup. The analysis included all 16 reference species and two sacoglossan species, and an expanded
748 group of 38 was determined on the PoB lineage (Threshold: Z-score > 2) (Supplementary Fig. 27). The
749 phylogenetic relationships in the orthogroups were also analyzed using a PREQUAL-MAFFT-IQ-tree. The

750 domain structures and gene positions on the constructed genome data were visualized using the GeneHere script
751 (<https://github.com/maedat/GeneHere>) and Biopython packages.
752
753

754 **Author contributions:**

755 T.Maeda, S.T., and S.Shigenobu. conceived of and designed the experiments; T.Maeda, S.T., J.M.,
756 performed the photochemical and physiological experiments and analyses; T.Maeda, A.A., T.Y., S.Shimamura.,
757 Y.T., Y.N., K.T., T.T., Y.S., M.K., N.S., T.N., M.H., T. Maruyama, J.O., and S.Shigenobu performed the
758 genomic and transcriptomic experiments and analyses. T.Maeda and S.Shigenobu wrote the paper following
759 advice from other authors.

760

761 **Acknowledgment:**

762 We appreciate the incisive comments offered by Masayoshi Kawaguchi, Atsushi J. Nagano, and Kan
763 Tanaka. The sample collection was supported by Katsuhiko Tanaka, Tohru Iseto, Rie Nakano, and Hirose Euichi.
764 This work was supported by the MEXT/JSPS KAKENHI (grant numbers 16H06279, 25128713 and 22128001),
765 National Institute for Basic Biology (NIBB) Functional Genomics Facility, NIBB Data Integration and Analysis
766 Facility, and the Japan Advanced Plant Science Network. Computations were partially performed on the NIG
767 supercomputer at ROIS National Institute of Genetics.

768

769 **Competing Interests:**

770 The authors declare no competing financial interests.

771 **Data availability:**

772 All of the raw sequence data obtained in this research have been deposited in the DDBJ Sequence Read Archive
773 (DRA) under BioProject PRJDB4939, PRJDB3267, PRJDB10060, and PRJDB5024. All data collected in this
774 study that are summarized in the figures have been made available on FigShare, at
775 DOI: 10.6084/m9.figshare.12300869, 10.6084/m9.figshare.12301865, 10.6084/m9.figshare.12301277,
776 10.6084/m9.figshare.12311990, 10.6084/m9.figshare.12316163, 10.6084/m9.figshare.12316283,
777 10.6084/m9.figshare.12316868, 10.6084/m9.figshare.12316895, 10.6084/m9.figshare.12318947,
778 10.6084/m9.figshare.12318962, 10.6084/m9.figshare.12318974, 10.6084/m9.figshare.12318977,
779 10.6084/m9.figshare.12318989, 10.6084/m9.figshare.12318992, 10.6084/m9.figshare.12318998,
780 10.6084/m9.figshare.12319001, 10.6084/m9.figshare.12319424, 10.6084/m9.figshare.12319532,

781 10.6084/m9.figshare.12318920, 10.6084/m9.figshare.12319739, 10.6084/m9.figshare.12319736,
782 10.6084/m9.figshare.12319802, 10.6084/m9.figshare.12319826, 10.6084/m9.figshare.12319832,
783 10.6084/m9.figshare.12319844, 10.6084/m9.figshare.12318908, 10.6084/m9.figshare.12319853,
784 10.6084/m9.figshare.12319859, 10.6084/m9.figshare.12319862, 10.6084/m9.figshare.12319889,
785 10.6084/m9.figshare.12628709, and 10.6084/m9.figshare.12587954. The codes used to analyze HGT index
786 and to visualize gene distribution on scaffolds have been made available on
787 https://github.com/maedat/HGT_index_ca and <https://github.com/maedat/GeneHere>.

788

789

790 References

- 791 Acuña R, Padilla BE, Flórez-Ramos CP, Rubio JD, Herrera JC, Benavides P, Lee S-J, Yeats TH, Egan AN, Doyle JJ,
792 Rose JKC. 2012. Adaptive horizontal transfer of a bacterial gene to an invasive insect pest of coffee. *Proc Natl*
793 *Acad Sci U S A* **109**:4197–4202.
- 794 Anderson NG. 1970. Evolutionary significance of virus infection. *Nature* **227**:1346–1347.
- 795 Arber W. 2014. Horizontal gene transfer among bacteria and Its role in biological evolution. *Life (Basel)* **4**:217–224.
- 796 Arimoto A, Nishitsuji K, Higa Y, Arakaki N, Hisata K, Shinzato C, Satoh N, Shoguchi E. 2019. A siphonous
797 macroalgal genome suggests convergent functions of homeobox genes in algae and land plants. *DNA Res*
798 **26**:183–192.
- 799 Benes P, Vetvicka V, Fusek M. 2008. Cathepsin D--many functions of one aspartic protease. *Crit Rev Oncol Hematol*
800 **68**:12–28.
- 801 Bessho-Uehara M, Yamamoto N, Shigenobu S, Mori H, Kuwata K, Oba Y. 2020. Kleptoprotein bioluminescence:
802 Parapriacanthus fish obtain luciferase from ostracod prey. *Sci Adv* **6**:eaax4942.
- 803 Bhattacharya D, Pelletreau KN, Price DC, Sarver KE, Rumpho ME. 2013. Genome analysis of *Elysia chlorotica* egg
804 DNA provides no evidence for horizontal gene transfer into the germ line of this kleptoplastic mollusc. *Mol Biol*
805 *Evol* **30**:1843–1852.
- 806 Bishop NA, Lu T, Yankner BA. 2010. Neural mechanisms of ageing and cognitive decline. *Nature* **464**:529–535.
- 807 Boschetti C, Carr A, Crisp A, Eyres I, Wang-Koh Y, Lubzens E, Barraclough TG, Micklem G, Tunnacliffe A. 2012.
808 Biochemical diversification through foreign gene expression in bdelloid rotifers. *PLoS Genet* **8**:e1003035.
- 809 Boto Luis. 2014. Horizontal gene transfer in the acquisition of novel traits by metazoans. *Proceedings of the Royal*
810 *Society B: Biological Sciences* **281**:20132450.
- 811 Cai H, Li Q, Fang X, Li J, Curtis NE, Altenburger A, Shibata T, Feng M, Maeda T, Schwartz JA, Shigenobu S,
812 Lundholm N, Nishiyama T, Yang H, Hasebe M, Li S, Pierce SK, Wang J. 2019. A draft genome assembly of the
813 solar-powered sea slug *Elysia chlorotica*. *Sci Data* **6**:190022.
- 814 Capella-Gutiérrez S, Silla-Martínez JM, Gabaldón T. 2009. trimAl: a tool for automated alignment trimming in large-
815 scale phylogenetic analyses. *Bioinformatics* **25**:1972–1973.
- 816 Cartaxana P, Trampe E, Kühl M, Cruz S. 2017. Kleptoplast photosynthesis is nutritionally relevant in the sea slug
817 *Elysia viridis*. *Sci Rep* **7**:7714.
- 818 Chan CX, Vaysberg P, Price DC, Pelletreau KN, Rumpho ME, Bhattacharya D. 2018. Active host response to algal
819 symbionts in the sea slug *Elysia chlorotica*. *Mol Biol Evol* **35**:1706–1711.
- 820 Charron J-BF, Ouellet F, Houde M, Sarhan F. 2008. The plant Apolipoprotein D ortholog protects *Arabidopsis*
821 against oxidative stress. *BMC Plant Biol* **8**:86.
- 822 Christa G, Gould SB, Franken J, Vleugels M, Karmeinski D, Händeler K, Martin WF, Wägele H. 2014a. Functional
823 kleptoplasty in a limapontioidean genus: phylogeny, food preferences and photosynthesis in *Costasiella*, with a
824 focus on *C. ocellifera* (Gastropoda: Sacoglossa). *J Molluscan Stud* **80**:499–507.
- 825 Christa G, Händeler K, Kück P, Vleugels M, Franken J, Karmeinski D, Wägele H. 2015. Phylogenetic evidence for
826 multiple independent origins of functional kleptoplasty in Sacoglossa (Heterobranchia, Gastropoda). *Org Divers*
827 *Evol* **15**:23–36.
- 828 Christa G, Händeler K, Schäberle TF, König GM, Wägele H. 2014b. Identification of sequestered chloroplasts in
829 photosynthetic and non-photosynthetic sacoglossan sea slugs (Mollusca, Gastropoda). *Front Zool* **11**:15.
- 830 Christa G, Wescott L, Schäberle TF, König GM, Wägele H. 2013. What remains after 2 months of starvation?
831 Analysis of sequestered algae in a photosynthetic slug, *Plakobranchnus ocellatus* (Sacoglossa, Opisthobranchia),
832 by barcoding. *Planta* **237**:559–572.
- 833 Christa G, Zimorski V, Woehle C, Tielens AGM, Wägele H, Martin WF, Gould SB. 2014c. Plastid-bearing sea slugs
834 fix CO₂ in the light but do not require photosynthesis to survive. *Proc Biol Sci* **281**:20132493.
- 835 Conrad B, Antonarakis SE. 2007. Gene duplication: a drive for phenotypic diversity and cause of human disease.
836 *Annu Rev Genomics Hum Genet* **8**:17–35.
- 837 Crick F. 1970. Central dogma of molecular biology. *Nature* **227**:561–563.
- 838 Cruz S, Cartaxana P, Newcomer R, Dionísio G, Calado R, Seródio J, Pelletreau KN, Rumpho ME. 2015.
839 Photoprotection in sequestered plastids of sea slugs and respective algal sources. *Sci Rep* **5**:7904.
- 840 Curtis NE, Pierce SK, Massey SE, Schwartz J, Mangel TK. 2007. Newly metamorphosed *Elysia clarki* juveniles feed
841 on and sequester chloroplasts from algal species different from those utilized by adult slugs. *Marine Biology*
842 **150**:797–806.
- 843 Dehal P, Satou Y, Campbell RK, Chapman J, Degnan B, De Tomaso A, Davidson B, Di Gregorio A, Gelpke M,
844 Goodstein DM, Harafuji N, Hastings KEM, Ho I, Hotta K, Huang W, Kawashima T, Lemaire P, Martinez D,

- 845 Meinertzhagen IA, Nacula S, Nonaka M, Putnam N, Rash S, Saiga H, Satake M, Terry A, Yamada L, Wang H-G,
846 G, Awazu S, Azumi K, Boore J, Branno M, Chin-Bow S, DeSantis R, Doyle S, Francino P, Keys DN, Haga S,
847 Hayashi H, Hino K, Imai KS, Inaba K, Kano S, Kobayashi K, Kobayashi M, Lee B-I, Makabe KW, Manohar C,
848 Matassi G, Medina M, Mochizuki Y, Mount S, Morishita T, Miura S, Nakayama A, Nishizaka S, Nomoto H,
849 Ohta F, Oishi K, Rigoutsos I, Sano M, Sasaki A, Sasakura Y, Shoguchi E, Shin-i T, Spagnuolo A, Stainier D,
850 Suzuki MM, Tassy O, Takatori N, Tokuoka M, Yagi K, Yoshizaki F, Wada S, Zhang C, Hyatt PD, Larimer F,
851 Detter C, Doggett N, Glavina T, Hawkins T, Richardson P, Lucas S, Kohara Y, Levine M, Satoh N, Rokhsar DS.
852 2002. The draft genome of *Ciona intestinalis*: insights into chordate and vertebrate origins. *Science* **298**:2157–
853 2167.
- 854 de Vries J, Archibald JM. 2018. Plastid autonomy vs nuclear control over plastid function In: Chaw S-M, Jansen RK,
855 editors. *Advances in Botanical Research*. Academic Press. pp. 1–28.
- 856 de Vries J, Woehle C, Christa G, Wägele H, Tielens AGM, Jahns P, Gould SB. 2015. Comparison of sister species
857 identifies factors underpinning plastid compatibility in green sea slugs. *Proc Biol Sci* **282**.
858 doi:10.1098/rspb.2014.2519
- 859 Emms DM, Kelly S. 2015. OrthoFinder: solving fundamental biases in whole genome comparisons dramatically
860 improves orthogroup inference accuracy. *Genome Biol* **16**:157.
- 861 Evertsen J, Burghardt I, Johnsen G, Wägele H. 2007. Retention of functional chloroplasts in some sacoglossans from
862 the Indo-Pacific and Mediterranean. *Mar Biol* **151**:2159–2166.
- 863 Fan X, Qiao H, Xu D, Cao S, Ye N. 2014. Short-term retention of kleptoplasty from a green alga (*Bryopsis*) in the sea
864 slug *Placida* sp. YS001. *Biologia* **69**:635–643.
- 865 Farah J, Rappaport F, Choquet Y, Joliot P, Rochaix JD. 1995. Isolation of a *psaF*-deficient mutant of *Chlamydomonas*
866 *reinhardtii*: efficient interaction of plastocyanin with the photosystem I reaction center is mediated by the Psf
867 subunit. *EMBO J* **14**:4976–4984.
- 868 Fu L, Niu B, Zhu Z, Wu S, Li W. 2012. CD-HIT: accelerated for clustering the next-generation sequencing data.
869 *Bioinformatics* **28**:3150–3152.
- 870 Gautheret D, Lambert A. 2001. Direct RNA motif definition and identification from multiple sequence alignments
871 using secondary structure profiles. *Journal of Molecular Biology* **313**:1003–1011.
- 872 Geijtenbeek TBH, Gringhuis SI. 2009. Signalling through C-type lectin receptors: shaping immune responses. *Nat*
873 *Rev Immunol* **9**:465–479.
- 874 Gilyarov MS. 1983. Appropriation of functioning organelles of food organisms by phytophagous and predatory
875 opisthobranch mollusks as a specific category of food utilization. *Zh Obshch Biol* **44**:614–620.
- 876 Grabherr MG, Haas BJ, Yassour M, Levin JZ, Thompson DA, Amit I, Adiconis X, Fan L, Raychowdhury R, Zeng Q,
877 Chen Z, Mauceli E, Hacohen N, Gnirke A, Rhind N, di Palma F, Birren BW, Nusbaum C, Lindblad-Toh K,
878 Friedman N, Regev A. 2011. Full-length transcriptome assembly from RNA-Seq data without a reference
879 genome. *Nat Biotechnol* **29**:644–652.
- 880 Green BJ, Li WY, Manhart JR, Fox TC, Summer EJ, Kennedy RA, Pierce SK, Rumpho ME. 2000. Mollusc-algal
881 chloroplast endosymbiosis. Photosynthesis, thylakoid protein maintenance, and chloroplast gene expression
882 continue for many months in the absence of the algal nucleus. *Plant Physiol* **124**:331–342.
- 883 Greve C, Ruiz-Tagle Lui M, Sivalingam S, Ludwig KU, Wägele H, Donath A. 2017. The complete mitochondrial
884 genome of the “solar-powered” sea slug *Plakobranthus* cf. *ocellatus* (Heterobranchia: Panpulmonata:
885 Sacoglossa). *Mitochondrial DNA Part B* **2**:130–131.
- 886 Haas BJ, Salzberg SL, Zhu W, Pertea M, Allen JE, Orvis J, White O, Buell CR, Wortman JR. 2008. Automated
887 eukaryotic gene structure annotation using EVIDENCEModeler and the program to assemble spliced alignments.
888 *Genome Biol* **9**:R7.
- 889 Hackett JD, Maranda L, Yoon HS, Bhattacharya D. 2003. Phylogenetic evidence for the *Cryptophyte* origin of the
890 plastid of *Dinophysis* (Dinophysiales, Dinophyceae). *J Phycol* **39**:440–448.
- 891 Händeler K, Grzybowski YP, Han JW, Wägele H. 2009. Functional chloroplasts in metazoan cells - a unique
892 evolutionary strategy in animal life. *Front Zool* **6**:28.
- 893 Han JH, Klochkova TA, Han JW, Shim J, Kim GH. 2015. Transcriptome analysis of the short-term photosynthetic sea
894 slug *Placida dendritica*. *Algae* **30**:303–312.
- 895 Han MV, Thomas GWC, Lugo-Martinez J, Hahn MW. 2013. Estimating gene gain and loss rates in the presence of
896 error in genome assembly and annotation using CAFE 3. *Mol Biol Evol* **30**:1987–1997.
- 897 Hershey AD, Chase M. 1952. Independent functions of viral protein and nucleic acid in growth of bacteriophage. *J*
898 *Gen Physiol* **36**:39–56.
- 899 Hirose E. 2005. Digestive system of the sacoglossan *Plakobranthus ocellatus* (Gastropoda: Opisthobranchia): light-
900 and electron-microscopic observations with remarks on chloroplast retention. *Zoolog Sci* **22**:905–916.
- 901 Hoff KJ, Lomsadze A, Borodovsky M, Stanke M. 2019. Whole-genome annotation with BRAKER. *Methods Mol Biol*
902 **1962**:65–95.
- 903 Huson DH, Auch AF, Qi J, Schuster SC. 2007. MEGAN analysis of metagenomic data. *Genome Res* **17**:377–386.

- 904 Izumi M, Tsunoda H, Suzuki Y, Makino A, Ishida H. 2012. RBCS1A and RBCS3B, two major members within the
905 *Arabidopsis* RBCS multigene family, function to yield sufficient Rubisco content for leaf photosynthetic
906 capacity. *J Exp Bot* **63**:2159–2170.
- 907 Jones P, Binns D, Chang HY, Fraser M, Li WZ, McAnulla C, McWilliam H, Maslen J, Mitchell A, Nuka G, Pesseat
908 S, Quinn AF, Sangrador-Vegas A, Scheremetjew M, Yong SY, Lopez R, Hunter S. 2014. InterProScan 5:
909 genome-scale protein function classification. *Bioinformatics* **30**:1236–1240.
- 910 Kajitani R, Toshimoto K, Noguchi H, Toyoda A, Ogura Y, Okuno M, Yabana M, Harada M, Nagayasu E, Maruyama
911 H, Kohara Y, Fujiyama A, Hayashi T, Itoh T. 2014. Efficient de novo assembly of highly heterozygous genomes
912 from whole-genome shotgun short reads. *Genome Res* **24**:1384–1395.
- 913 Kalvari I, Argasinska J, Quinones-Olvera N, Nawrocki EP, Rivas E, Eddy SR, Bateman A, Finn RD, Petrov AI. 2018.
914 Rfam 13.0: shifting to a genome-centric resource for non-coding RNA families. *Nucleic Acids Res* **46**:D335–
915 D342.
- 916 Katoh K, Standley DM. 2013. MAFFT multiple sequence alignment software version 7: improvements in
917 performance and usability. *Mol Biol Evol* **30**:772–780.
- 918 Kawaguti. 1965. Electron microscopy on the symbiosis between an elysiid gastropod and chloroplasts of a green
919 alga. *Biol J Okuyama Univ* **11**:57–65.
- 920 Kawaguti S. 1941. Study on the invertebrates associating unicellular algae I. *Placobranchus ocellatus* von Hasselt, a
921 nudibranch. *Palau Tropical Biological Station Studies* **2**.
- 922 Kim D, Pertea G, Trapnell C, Pimentel H, Kelley R, Salzberg SL. 2013. TopHat2: accurate alignment of
923 transcriptomes in the presence of insertions, deletions and gene fusions. *Genome Biol* **14**:R36.
- 924 Krug PJ, Vendetti JE, Rodriguez AK, Retana JN, Hirano YM, Trowbridge CD. 2013. Integrative species delimitation
925 in photosynthetic sea slugs reveals twenty candidate species in three nominal taxa studied for drug discovery,
926 plastid symbiosis or biological control. *Mol Phylogenet Evol* **69**:1101–1119.
- 927 Laetz EMJ, Wägele H. 2018. Comparing amylose production in two solar-powered sea slugs: the sister taxa *Elysia*
928 *timida* and *E. cornigera* (Heterobranchia: Sacoglossa). *J Molluscan Stud.* doi:10.1093/mollus/eyy047
- 929 Laetz EMJ, Wägele H. 2017. Chloroplast digestion and the development of functional kleptoplasty in juvenile *Elysia*
930 *timida* (Risso, 1818) as compared to short-term and non-chloroplast-retaining sacoglossan slugs. *PLoS One*
931 **12**:e0182910.
- 932 Langmead B, Salzberg SL. 2012. Fast gapped-read alignment with Bowtie 2. *Nat Methods* **9**:357–359.
- 933 Lis H, Sharon N. 1998. Lectins: carbohydrate-specific proteins that mediate cellular recognition. *Chem Rev* **98**:637–
934 674.
- 935 Maeda T, Hirose E, Chikaraishi Y, Kawato M, Takishita K, Yoshida T, Verbruggen H, Tanaka J, Shimamura S,
936 Takaki Y, Tsuchiya M, Iwai K, Maruyama T. 2012. Algivore or phototroph? *Plakobranchus ocellatus*
937 (Gastropoda) continuously acquires kleptoplasts and nutrition from multiple algal species in nature. *PLoS One*
938 **7**:e42024.
- 939 Magoc T, Salzberg SL. 2011. FLASH: fast length adjustment of short reads to improve genome assemblies.
940 *Bioinformatics* **27**:2957–2963.
- 941 Majoros WH, Pertea M, Salzberg SL. 2004. TigrScan and GlimmerHMM: two open source *ab initio* eukaryotic gene-
942 finders. *Bioinformatics* **20**:2878–2879.
- 943 Martin R, Walther P, Tomaschko K-H. 2015. Variable retention of kleptoplast membranes in cells of sacoglossan sea
944 slugs: plastids with extended, shortened and non-retained durations. *Zoomorphology* **134**:523–529.
- 945 Meyers-Muñoz MA, van der Velde G, van der Meij SET, Stoffels BEMW, van Alen T, Tuti Y, Hoeksema BW. 2016.
946 The phylogenetic position of a new species of *Plakobranchus* from west Papua, Indonesia (Mollusca,
947 Opisthobranchia, Sacoglossa). *Zookeys* **73**–98.
- 948 Murray MG, Thompson WF. 1980. Rapid isolation of high molecular weight plant DNA. *Nucleic Acids Res* **8**:4321–
949 4325.
- 950 O'Connor RM, Fung JM, Sharp KH, Benner JS, McClung C, Cushing S, Lamkin ER, Fomenkov AI, Henrissat B,
951 Londer YY, Scholz MB, Posfai J, Malfatti S, Tringe SG, Woyke T, Malmstrom RR, Coleman-Derr D, Altamia
952 MA, Dedrick S, Kaluziak ST, Haygood MG, Distel DL. 2014. Gill bacteria enable a novel digestive strategy in a
953 wood-feeding mollusk. *Proc Natl Acad Sci U S A* **111**:E5096–104.
- 954 Pelletreau KN, Bhattacharya D, Price DC, Worful JM, Moustafa A, Rumpho ME. 2011. Sea slug kleptoplasty and
955 plastid maintenance in a metazoan. *Plant Physiol* **155**:1561–1565.
- 956 Pierce S, Biron R, Rumpho M. 1996. Endosymbiotic chloroplasts in molluscan cells contain proteins synthesized after
957 plastid capture. *J Exp Biol* **199**:2323–2330.
- 958 Pierce SK, Curtis NE. 2012. Cell biology of the chloroplast symbiosis in sacoglossan sea slugs. *Int Rev Cell Mol Biol*
959 **293**:123–148.
- 960 Pierce SK, Curtis NE, Hanten JJ, Boerner SL, Schwartz J. 2007. Transfer, integration and expression of functional
961 nuclear genes between multicellular species. *Symbiosis* **43**:57–64.
- 962 Pierce SK, Curtis NE, Schwartz J. 2010. Chlorophyll a synthesis by an animal using transferred algal nuclear genes.

- 963 *Symbiosis* **49**:121–131.
- 964 Pierce SK, Massey SE, Hanten JJ, Curtis NE. 2003. Horizontal transfer of functional nuclear genes between
965 multicellular organisms. *Biol Bull* **204**:237–240.
- 966 Pigolev AV, Zharmukhamedov SK, Klimov VV. 2009. The *psbO* mutant of *Chlamydomonas reinhardtii* is capable of
967 assembling stable, photochemically active reaction center of photosystem II. *Biochemistry (Moscow) Supplement*
968 *Series A: Membrane and Cell Biology* **3**:33–41.
- 969 Rauch C, Vries J de, Rommel S, Rose LE, Woehle C, Christa G, Laetz EM, Wägele H, Tielens AGM, Nickelsen J,
970 Schumann T, Jahns P, Gould SB. 2015. Why it is time to look beyond algal genes in photosynthetic slugs.
971 *Genome Biol Evol* **7**:2602–2607.
- 972 Reyes-Prieto A, Weber APM, Bhattacharya D. 2007. The origin and establishment of the plastid in algae and plants.
973 *Annu Rev Genet* **41**:147–168.
- 974 Roberts IN, Miranda H, Tãm LX, Kieselbach T, Funk C. 2013. PsbO degradation by Deg proteases under reducing
975 conditions In: Kuang T, Lu C, Zhang L, editors. Photosynthesis Research for Food, Fuel and the Future. Springer
976 Berlin Heidelberg. pp. 599–602.
- 977 Rumpho ME, Pelletreau KN, Moustafa A, Bhattacharya D. 2011. The making of a photosynthetic animal. *J Exp Biol*
978 **214**:303–311.
- 979 Rumpho ME, Worful JM, Lee J, Kannan K, Tyler MS, Bhattacharya D, Moustafa A, Manhart JR. 2008. Horizontal
980 gene transfer of the algal nuclear gene *psbO* to the photosynthetic sea slug *Elysia chlorotica*. *Proc Natl Acad Sci*
981 *U S A* **105**:17867–17871.
- 982 Sanderson MJ. 2003. r8s: inferring absolute rates of molecular evolution and divergence times in the absence of a
983 molecular clock. *Bioinformatics* **19**:301–302.
- 984 Sasakura Y, Ogura Y, Treen N, Yokomori R, Park S-J, Nakai K, Saiga H, Sakuma T, Yamamoto T, Fujiwara S,
985 Yoshida K. 2016. Transcriptional regulation of a horizontally transferred gene from bacterium to chordate. *Proc*
986 *Biol Sci* **283**. doi:10.1098/rspb.2016.1172
- 987 Schwartz JA, Curtis NE, Pierce SK. 2014. FISH labeling reveals a horizontally transferred algal (*Vaucheria litorea*)
988 nuclear gene on a sea slug (*Elysia chlorotica*) chromosome. *Biol Bull* **227**:300–312.
- 989 Serôdio J, Cruz S, Cartaxana P, Calado R. 2014. Photophysiology of kleptoplasts: photosynthetic use of light by
990 chloroplasts living in animal cells. *Philos Trans R Soc Lond B Biol Sci* **369**:20130242.
- 991 Slater GS, Birney E. 2005. Automated generation of heuristics for biological sequence comparison. *BMC*
992 *Bioinformatics* **6**. doi:Artn 31 10.1186/1471-2105-6-31
- 993 Stamatakis A. 2014. RAxML version 8: a tool for phylogenetic analysis and post-analysis of large phylogenies.
994 *Bioinformatics* **30**:1312–1313.
- 995 Stanke M, Morgenstern B. 2005. AUGUSTUS: a web server for gene prediction in eukaryotes that allows user-
996 defined constraints. *Nucleic Acids Res* **33**:W465–7.
- 997 Taylor DL. 1968. Chloroplasts as symbiotic organelles in the digestive gland of *Elysia viridis* (Gastropoda:
998 opisthobranchia). *J Mar Biol Assoc U K* **48**:1–15.
- 999 Ter-Hovhannisyán V, Lomsadze A, Chernoff YO, Borodovsky M. 2008. Gene prediction in novel fungal genomes
1000 using an *ab initio* algorithm with unsupervised training. *Genome Res* **18**:1979–1990.
- 1001 Teugels B, Bouillon S, Veuger B, Middelburg JJ, Koedam N. 2008. Kleptoplasts mediate nitrogen acquisition in the
1002 sea slug *Elysia viridis*. *Aquatic Biology* **4**:15–21.
- 1003 Trench ME, Trench RK, Muscatine L. 1970. Utilization of photosynthetic products of symbiotic chloroplasts in
1004 mucus synthesis by *Placobranchus ianthobapsus* (Gould), Opisthobranchia, Sacoglossa. *Comparative*
1005 *Biochemistry and Physiology* **37**:113–117.
- 1006 Trench RK. 1969. Chloroplasts as functional endosymbionts in the mollusc *Tridachia crispata* (Bérgh),
1007 (Opisthobranchia, Sacoglossa). *Nature* **222**:1071.
- 1008 Wade RM, Sherwood AR. 2017. Molecular determination of kleptoplast origins from the sea slug *Plakobranchus*
1009 *ocellatus* (Sacoglossa, Gastropoda) reveals cryptic bryopsidalean (Chlorophyta) diversity in the Hawaiian
1010 Islands. *J Phycol* **53**:467–475.
- 1011 Wägele H, Deusch O, Händeler K, Martin R, Schmitt V, Christa G, Pinzger B, Gould SB, Dagan T, Klusmann-Kolb
1012 A, Martin W. 2011. Transcriptomic evidence that longevity of acquired plastids in the photosynthetic slugs
1013 *Elysia timida* and *Plakobranchus ocellatus* does not entail lateral transfer of algal nuclear genes. *Mol Biol Evol*
1014 **28**:699–706.
- 1015 Wägele M, Johnsen G. 2001. Observations on the histology and photosynthetic performance of “solar-powered”
1016 opisthobranchs (Mollusca, Gastropoda, Opisthobranchia) containing symbiotic chloroplasts or zooxanthellae.
1017 *Org Divers Evol* **1**:193–210.
- 1018 Waterhouse RM, Seppey M, Simão FA, Manni M, Ioannidis P, Klioutchnikov G, Kriventseva EV, Zdobnov EM.
1019 2018. BUSCO applications from quality assessments to gene prediction and phylogenomics. *Mol Biol Evol*
1020 **35**:543–548.
- 1021 Watson JD, Crick FH. 1953. Molecular structure of nucleic acids; a structure for deoxyribose nucleic acid. *Nature*

- 1022 171:737–738.
- 1023 Whelan S, Irisarri I, Burki F. 2018. PREQUAL: detecting non-homologous characters in sets of unaligned
- 1024 homologous sequences. *Bioinformatics* **34**:3929–3930.
- 1025 Wickner RB, Shewmaker FP, Bateman DA, Edskes HK, Gorkovskiy A, Dayani Y, Bezsonov EE. 2015. Yeast prions:
- 1026 structure, biology, and prion-handling systems. *Microbiol Mol Biol Rev* **79**:1–17.
- 1027 Worthley DL, Bardy PG, Mullighan CG. 2005. Mannose-binding lectin: biology and clinical implications. *Intern Med*
- 1028 *J* **35**:548–555.
- 1029 Yamamoto S, Hirano YM, Hirano YJ, Trowbridge CD, Akimoto A, Sakai A, Yusa Y. 2013. Effects of photosynthesis
- 1030 on the survival and weight retention of two kleptoplastic sacoglossan opisthobranchs. *J Mar Biol Assoc U K*
- 1031 **93**:209–215.
- 1032 Yamamoto YY, Yusa Y, Yamamoto S, Hirano Y, Hirano Y, Motomura T, Tanemura T, Obokata J. 2009.
- 1033 Identification of photosynthetic sacoglossans from Japan. *Encocytobiosis Cell Res* **19**:112.
- 1034 Yamasaki S, Ishikawa E, Sakuma M, Hara H, Ogata K, Saito T. 2008. Mincle is an ITAM-coupled activating receptor
- 1035 that senses damaged cells. *Nat Immunol* **9**:1179–1188.
- 1036 Young MD, Wakefield MJ, Smyth GK, Oshlack A. 2010. Gene ontology analysis for RNA-seq: accounting for
- 1037 selection bias. *Genome Biol* **11**:R14.
- 1038 Zapata F, Wilson NG, Howison M, Andrade SCS, Jörger KM, Schrödl M, Goetz FE, Giribet G, Dunn CW. 2014.
- 1039 Phylogenomic analyses of deep gastropod relationships reject Orthogastropoda. *Proc Biol Sci* **281**:20141739.
- 1040 Zerbino DR, Birney E. 2008. Velvet: algorithms for de novo short read assembly using *de Bruijn* graphs. *Genome Res*
- 1041 **18**:821–829.
- 1042 Zuker M. 2003. Mfold web server for nucleic acid folding and hybridization prediction. *Nucleic Acids Res* **31**:3406–
- 1043 3415.
- 1044
- 1045
- 1046
- 1047

1048 **Figure legends**

1049 **Fig. 1. Kleptoplasty in sea slugs.**

1050 **a** The process of algal chloroplast retention by a sacoglossan sea slug (Pierce and Curtis, 2012). **b–d**
1051 Images of *P. ocellatus* type black starved for 21 days. **b** Dorsal view. **c** Spread parapodia. H, head; P,
1052 parapodium; DG, digestive gland. **d** Enlarged view of the surface of the parapodium and digestive gland.
1053 Kleptoplasts are visible as a green color. **e** Phylogenetic distribution of kleptoplasty in the order
1054 Sacoglossa. Phylogenetic tree and kleptoplasty states are simplified from Christa et al. (2015).
1055 Relationships within Heterobranchia are described based on Zapata et al. (2014). **f** Phylogeny of the *P. cf.*
1056 *ocellatus* species complex based on mitochondrial *coxI* genes (Maximum Likelihood tree from 568
1057 nucleotide positions) from INSDC and our whole mitochondrial DNA sequence. Clade names in square
1058 brackets are based on Krug et al. (2013). Asterisks mark genotypes from Krug et al. (2013). Previously
1059 analyzed topics for each cluster are described within the colored boxes. Small black circles indicate nodes
1060 supported by a high bootstrap value (i.e., 80%–100%). *Thuridilla gracilis* is outgroup. *Plakobranchus*
1061 *papua* is recently described species and previously identified as *P. ocellatus* (Meyers-Muñoz et al., 2016).
1062 The detailed data for the samples were registered in FigShare (DOI, 10.6084/m9.figshare.12300869)

1063

1064 **Fig. 2. Photosynthetic activity of *P. ocellatus* type black**

1065 **a** Jitter plot of Fv/Fm values indicating the photochemical efficiency of photosystem II. Habo, *H.*
1066 *borneensis*; PoB, *P. ocellatus* type black; d38, starved for 38 days; d109, starved for 109–110 day (12
1067 h:12 h light-dark cycle, the light phase illumination was 10 $\mu\text{mol photons m}^{-2} \text{s}^{-1}$). Magenta line indicates
1068 the mean value, black dot indicates the raw value of each individual ($n = 3$, each group). **b** Time-course of
1069 oxygen concentration in the water in which PoB was reared. Gray color signifies a dark period; yellow
1070 color signifies an illuminated period (50 $\mu\text{mol photons m}^{-2} \text{s}^{-1}$). Temp, water temperature. **c** Jitter plots of
1071 PoB oxygen consumption and generation. D, dark condition; L, light condition; G, gross rate of light-
1072 dependent oxygen generation (L minus D). **d** Jitter plots of PoB longevity ($n = 5$, each group). D,

1073 Continuous dark; L/D, 12 h:12 h light-dark cycle. The *p*-value from Welch's two-sample *t*-test is shown.
1074 Raw data, Supplementary Table 1.

1075

1076 **Fig. 3. Gene composition of *P. ocellatus* type black kleptoplast DNAs**

1077 **a** Gene map of two kleptoplast DNAs from PoB. Gene positions are described in circles colored
1078 according to the functional category of the gene (see key). Genes on the outside and inside of each circle
1079 are transcribed in the clockwise and anticlockwise direction, respectively (for detailed maps, see
1080 Supplementary Figs. 2 and 3). **b** Phylogenetic positions of sequenced kleptoplasts among green algal
1081 plastids. The tree was simplified from an ML tree based on *rbcL* genes (457 positions). When multiple
1082 sequences derived from the same species were registered in the INSDC due to intra-species variation,
1083 these multiple sequences were included in the analysis (original tree: Supplementary Fig. 5). Red color
1084 indicates sequenced kpDNA or cpDNA in the present study. Underlining indicates algal species used for
1085 our RNA-Seq sequencing. **c** An UpSet plot of plastid gene composition. Species abbreviations are defined
1086 in Supplementary Table 3. The horizontal bar chart indicates the gene numbers in each species. The
1087 vertical bar chart indicates the number of genes conserved among the species. Intersect connectors
1088 indicate species composition in which a given number of genes (vertical bar chart). We omitted
1089 connections corresponding to no gene. Connectors are colored according to the conservation level of the
1090 gene (see key): Core gene, conserved among all of the analyzed Bryopsidales species; Dispensable gene,
1091 retained over 2 Bryopsidales species; Rare gene, determined from a single or no Bryopsidales species.
1092 Gray shading indicates non-Viridiplantae algae, and magenta shading indicates PoB kleptoplasts. **d** Box
1093 plots of tblastn results. The y-axis shows the database searched (kPoro and kRhip, PoB kleptoplast
1094 DNAs; nCale, nucDNA of *Caulerpa lentillifera*). Each dot represents the tblastn result (query is A614
1095 dataset). Red dots show the result using the *chlD* gene (encoding Magnesium-chelatase subunit ChlD) as
1096 the query sequence; this sequence is similar to the kleptoplast-encoded *chlL* gene. The right pie chart
1097 shows the proportion of queries with hits (E-value <0.0001). **e** Heat map of tblastn results of
1098 representative photosynthetic nuclear genes (a subset of data in Fig. 3d). The source species of the query
1099 sequences are described on the top: Abbreviations are defined in Supplementary Table 3. Raw data: DOI

1100 10.6084/m9.figshare.12311990, 10.6084/m9.figshare.12316163, 10.6084/m9.figshare.12318962, and
1101 10.6084/m9.figshare.12318974.

1102

1103 **Fig. 4 Search for horizontally transferred algal-genes in the *P. ocellatus* type black genome**

1104 **a** Heatmap of gene ontology (GO) comparison analysis among PoB, two non-kleptoplastic mollusk
1105 species (*Aca*, *Aplysia californica*; *Bgl*, *Biomphalaria glabrata*), and 5 algae species (abbreviations as
1106 defined in Supplementary Table 3). For each species, the number of genes assigned to various
1107 photosynthesis- or plastid-related GO terms are visualized on a color scale (see key). **b** Scatter plot of the
1108 results of the alignment of the A614 gene set (query sequences) of photosynthetic genes to the PoB
1109 genome using Exonerate software. The enlarged view is shown on Supplementary Fig. 17 with tblastn
1110 result). The dot color shows the source algae of each query sequence (see key). The horizontal axis shows
1111 what percentage of the query sequences were aligned to the hit sequences (PoB genome). The vertical
1112 axis shows the similarity of the aligned sequences between the query and PoB genome; alignment score
1113 (the sum of the substitution matrix scores and the gap penalties) divided by aligned length (bp). Dashed
1114 lines are thresholds for a credible query hit (i.e., a hit covering >60% of the query sequence, and a
1115 normalized Exonerate alignment score of >2). **c** Scatter plot of MMseq2 results for the A614 dataset
1116 (algal photosynthetic genes, red) and P911 reference dataset (PoB single-copy genes, blue) used as query
1117 sequences against our database of preassembled read sets from paired-end DNA libraries of PoB. The
1118 upper panel shows the probability density distribution of the number of hit-reads (normalized with TPM:
1119 transcripts per kilobase million) (x-axis) versus averaged “pident” value (percentage of identical matches)
1120 from the hit reads (y-axis). **d** Scatter plot of HGT indexes (hA- versus h-index) for genes in PoB, the two
1121 non-kleptoplastic mollusk species (*Aca* and *Bgl*), and one algae species (*Caulerpa lentillifera* [*Cale*]).
1122 Each dot represents a gene. A high hA or h-index value means the possibility of algal or prokaryote origin,
1123 respectively. Dashed red lines represent the conventional threshold for HGT (-100 for h index and 100 for
1124 hA index). **e** Heatmap of the results of searches for algae-like RNA fragments in the PoB RNA-Seq data.
1125 DG, digestive gland; Pa, parapodia; DeP, DG-exenterated parapodia; EG, egg; He, head; Pe, pericardium.
1126 The blue color gradient indicates the number of RNA-Seq reads assigned as algae-like fragments (see
1127 key). The y-axis labels show the RNA-Seq library name and analyzed tissue types (see Supplementary

1128 Fig. 21). The x-axis labels indicate the query protein; those with no corresponding RNA reads were
1129 omitted from the figure. For queries using the P911 reference dataset, we describe the mean value of the
1130 hit-read counts from each library. The total number of reads for each library is given on the far right.
1131 Detailed and raw data: Supplementary Figs. 14–21, 10.6084/m9.figshare.12318920,
1132 10.6084/m9.figshare.12319739, and 10.6084/m9.figshare.12319736.

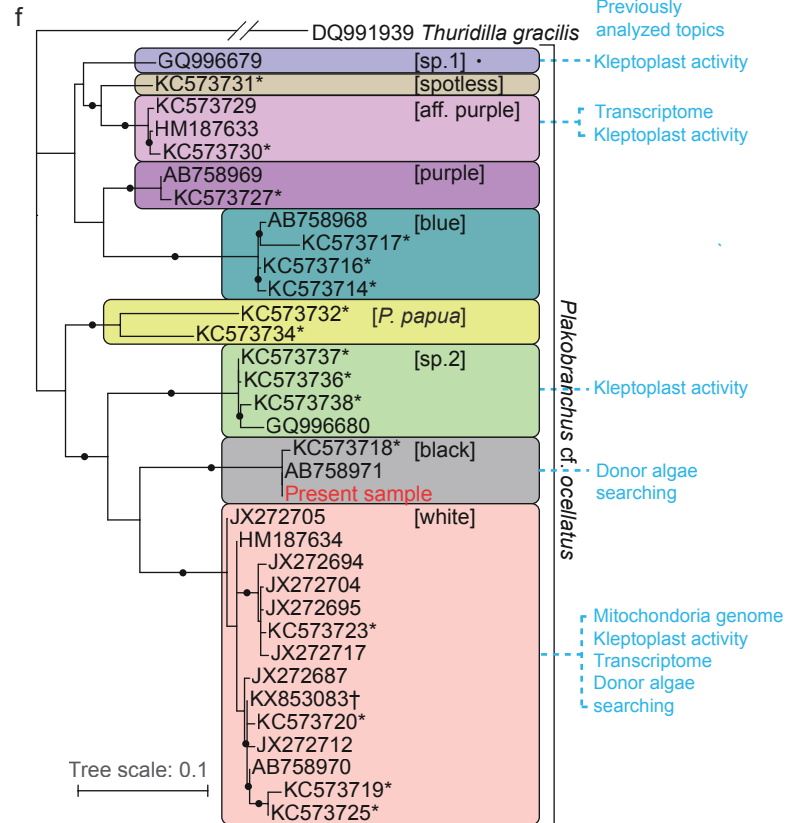
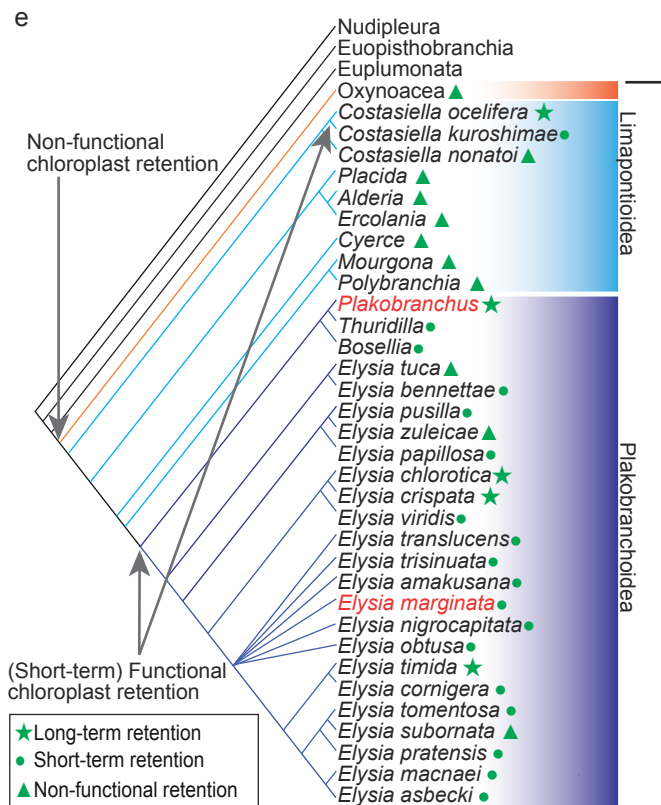
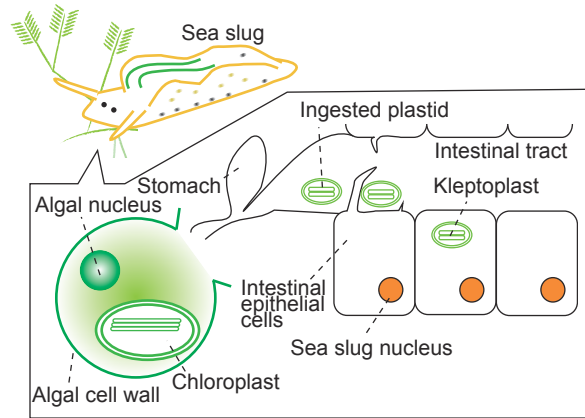
1133

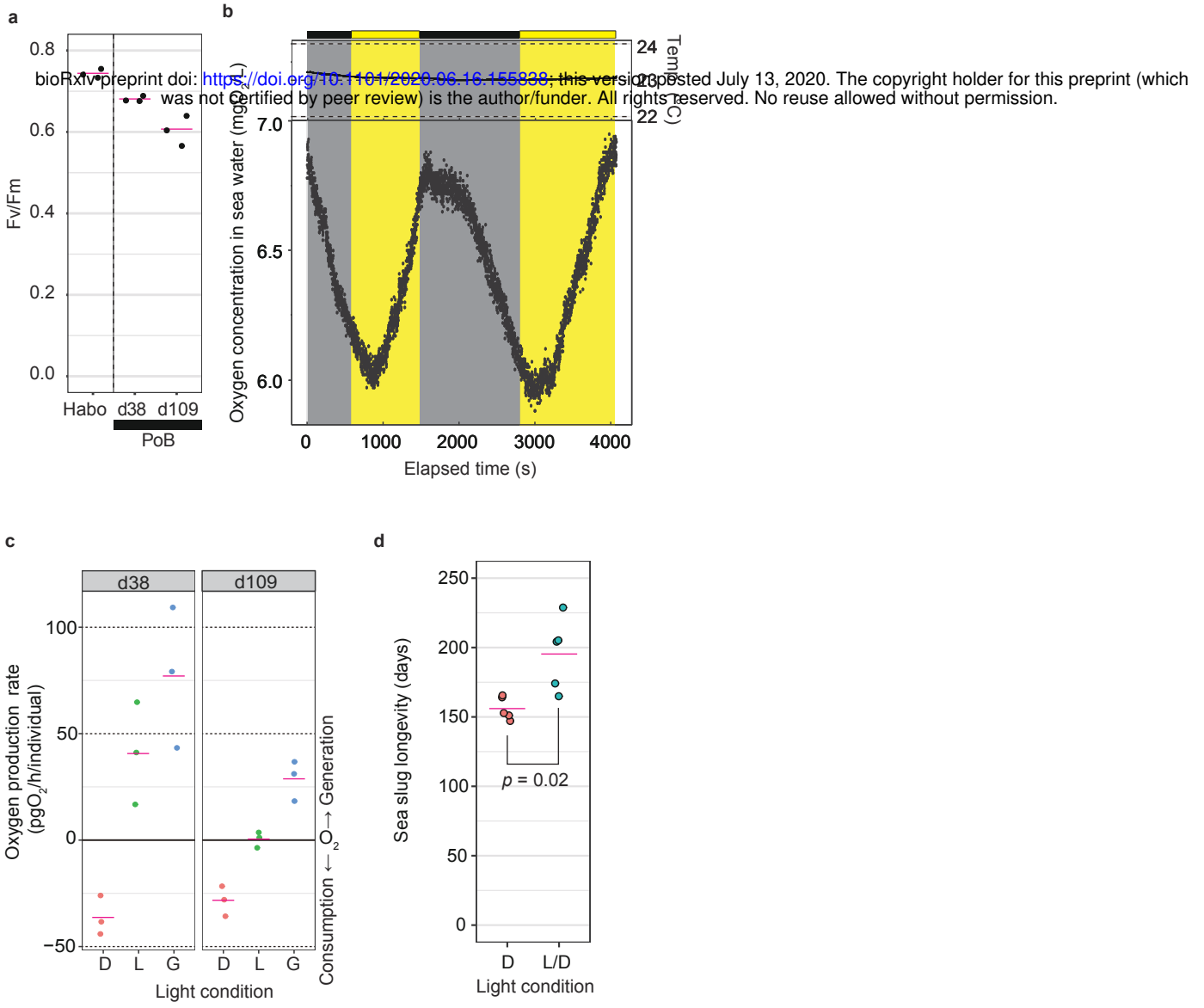
1134 **Fig. 5 Probable kleptoplasty-related molluscan genes in *P. ocellatus* type black**

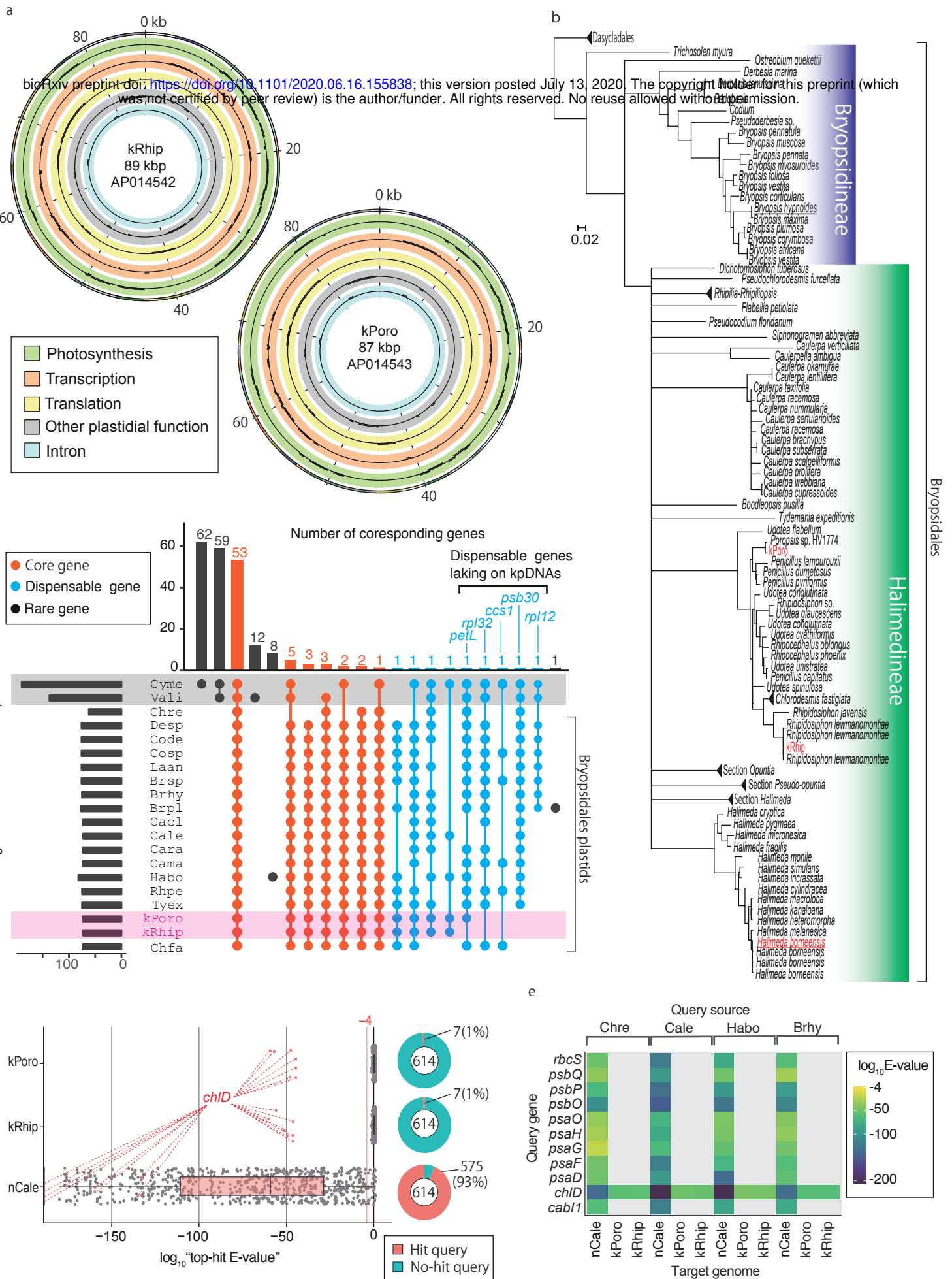
1135 **a** Volcano plot comparing gene expression in the digestive gland (DG) and DG-exenterated parapodia
1136 (DeP) tissue of PoB. Red indicates orthogroup OG0000132 (cathepsin D-like protease genes); blue
1137 indicates orthogroup OG0000005 (lectin-like genes); and orange indicates other orthogroups (for details,
1138 see Supplementary Fig. 25). Up and down arrows signify up- and down-regulated, respectively, in DG. **b**
1139 Orthogroups that were expanded on the *P. ocellatus* lineage and contained DG-upregulated genes. PoB, *P.*
1140 *ocellatus* type black; Ema, *E. marginata*; Bgl, *Biomphalaria glabrata*; Lgi, *Lottia gigantea*; Hdi, *Haliotis*
1141 *discus*; Obi, *Octopus bimaculoides*; Pfu, *Pinctada fucata*; Cgi, *Crassostrea gigas*; Cte, *Capitella teleta*;
1142 Dme, *Drosophila melanogaster*; Bmo, *Bombyx mori*; Api, *Acyrtosiphon pisum*; Hsa, *Homo sapiens*;
1143 Mmu, *Mus musculus*. The phylogenetic tree is scaled to divergence time based on 30 conserved single-
1144 copy genes. Mya = million years. The numbers of rapidly expanded (blue) and contracted (magenta)
1145 orthogroups on the lineages to PoB are provided at the nodes (Detail data: Supplementary Fig. 24). Below
1146 the tree is information for the six expanded orthogroups that contained DG-upregulated genes. The left-
1147 side heatmap shows the gene numbers (number in boxes) and z-score of gene numbers (color gradient) for
1148 each orthogroup. The table shows the expanded/not expanded status of each orthogroup (P–E,
1149 *Plakobranchus–Elysia* node; Poc, *Plakobranchus* node) (for details, see Supplementary Figs. 26 and 27).
1150 The right-side heat map indicates the number of differentially expressed genes (DEGs) between DG and
1151 DeP tissue in each orthogroup. Representative gene products are given on the far right.. **c** Details for
1152 OG0000132 (phylogeny, domain structure, gene expression, and gene positions on the assemblies). The
1153 phylogenetic tree on the far left is a part of the ML tree for OG0000132 genes (Supplementary Fig. 28).
1154 Red circles mark PoB genes; blue squares mark *E. marginata* (Ema) genes. Other species are represented
1155 with pictograms defined in Supplementary Table 14. The domain structure of the proteins encoded by

1156 OG0000132 genes is shown in the centre left (see “Domain structure” key on far right). The expression of
1157 each gene in OG0000132 in various tissues is shown in the centre right; tissue abbreviations are as
1158 defined in the Fig. 4 legend (see “Gene expression” key on far right). Genes derived from organisms other
1159 than PoB are shown in gray. The false discovery rate (FDR) was calculated by the comparison between
1160 DG and DeP samples. Genes for which no expression was observed on DG nor DeP (FDR could not be
1161 calculated) are shown in black. In the right panel, the genomic positions of OG0000132 genes on
1162 scaffolds are shown as red boxes, and other protein-encoding genes are shown as blue boxes. Purple text
1163 and arrows indicate the scaffold ID and direction, respectively. The color of the bands indicates the
1164 correlation between the gene and position. Scaffolds having less than 5 genes belonging to OG0000132
1165 were omitted from the figure. Raw data: DOI 10.6084/m9.figshare.12319802,
1166 10.6084/m9.figshare.12319826, 10.6084/m9.figshare.12319832, 10.6084/m9.figshare.12319844,
1167 10.6084/m9.figshare.12318908, 10.6084/m9.figshare.12319853 10.6084/m9.figshare.12319859, and
1168 10.6084/m9.figshare.12319862

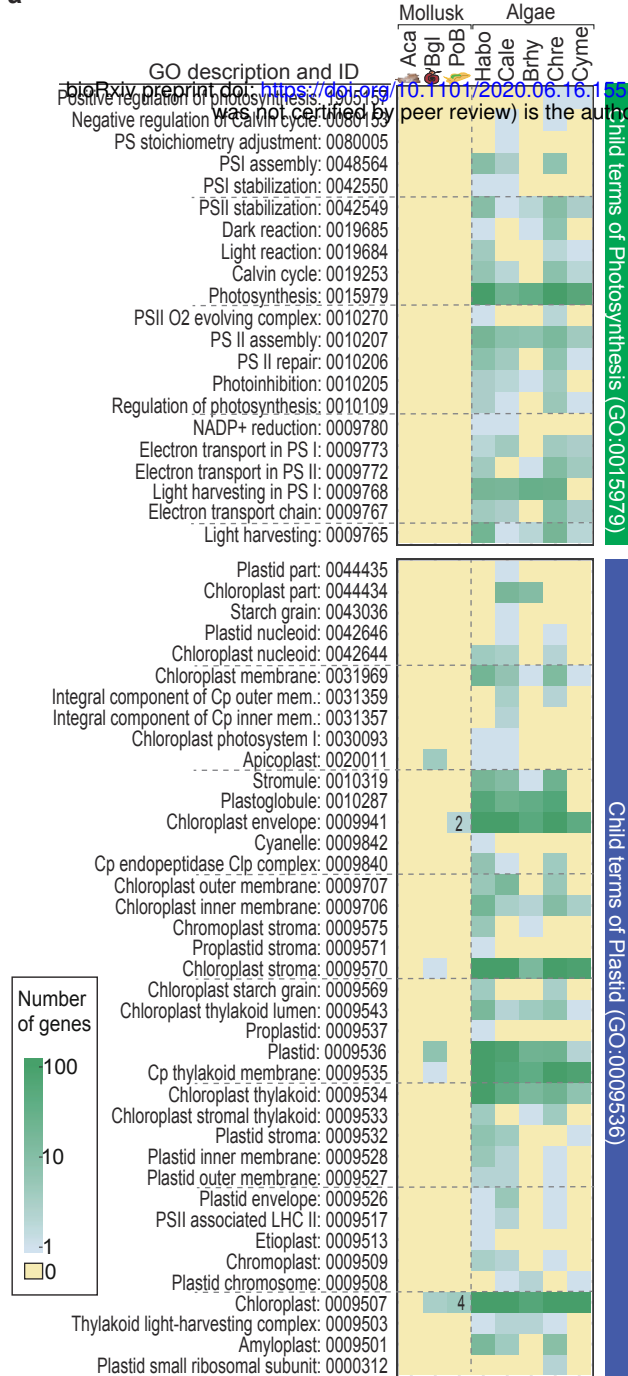
a Food algae



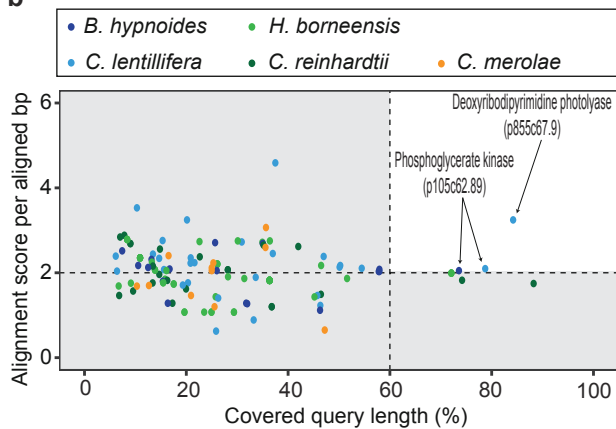




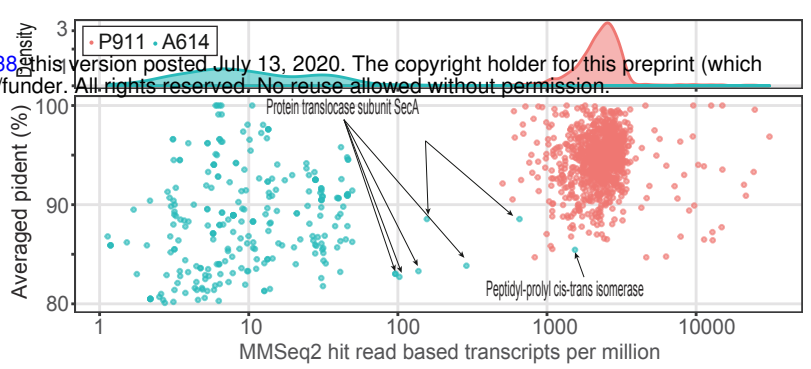
a



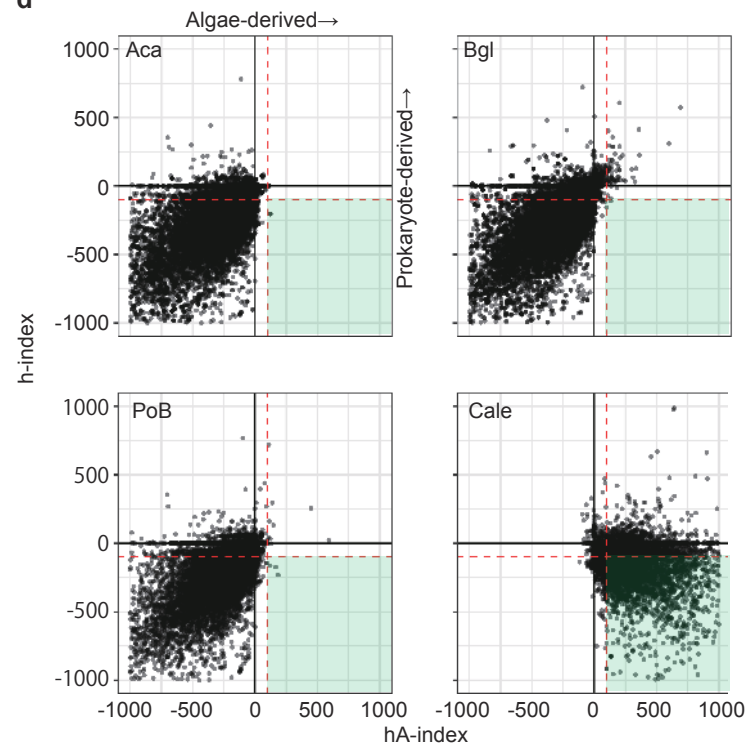
b



c



d



e

